Neurophysiological brain-fingerprints of motor and cognitive decline in Parkinson's disease

Jason da Silva Castanheira[1], Alex I. Wiesman[1], Justine Y. Hansen[1], Bratislav Misic[1], Sylvain Baillet[1,†], PREVENT-AD Research Group[‡], Quebec Parkinson Network.

[1] Montreal Neurological Institute, McGill University, Montreal QC, Canada
[†] Corresponding author: sylvain.baillet@mcgill.ca.

[‡]Data used in preparation of this article were obtained from the Pre-symptomatic Evaluation of Novel or Experimental Treatments for Alzheimer's Disease (PREVENT-AD) program (https://douglas.research.mcgill.ca/stop-ad-centre), data release 6.0. A complete listing of PREVENT-AD Research Group can be found in the PREVENT-AD database: https://preventad.loris.ca/acknowledgements/acknowledgements.php?date=[2022-02-01]. The investigators of the PREVENT-AD program contributed to the design and implementation of PREVENT-AD and/or provided data but did not participate in analysis or writing of this report.

Abstract

Brain-fingerprinting is a neuroimaging approach that is expanding the neuroscientific perspective on inter-individual diversity in health and disease. In the present study, we used brain-fingerprinting to advance the neurophysiological characterization of Parkinson's disease (PD). We derived the brain-fingerprints of patients with PD and age-matched healthy controls from the rhythmic and arhythmic spectral features of brief and task-free magnetoencephalography recordings. Using this approach, the individual differentiation of patients against healthy controls is 81% accurate, with the differentiability of patients scaling with the severity of their cognitive and motor symptoms. We show that between-patient differentiation is more challenging (77% accurate) than between healthy controls (90%) because the neurophysiological spectral features of patients with PD are less stable over time. The most distinctive features for differentiating healthy controls map to higher-order regions in the brain functional hierarchy. In contrast, the most distinctive features for patient differentiation map to the somatosensori-motor cortex. We also report that patient brain-fingerprints coincide with the cortical topography of the neurotransmitter systems affected in PD. We conclude that Parkinson's disease affects the spectral brain-fingerprint of patients with remarkable heterogeneity between individuals, and increased variability over short periods of time, compared to age-matched healthy controls. Our study demonstrates the relevance of neurophysiological fingerprinting to clinical neuroscience, and highlights its potential in terms of patient stratification, disease modeling, and the development and evaluation of personalized interventions.

Lay summary:

Brain fingerprinting is a novel approach that advances the neuroscientific understanding of differences between individuals. Recent work has shown that brief recordings of our brain activity differentiate us from each other, just like the fingerprints of our hand. The present study investigates how brain-fingerprints can help evaluate patients affected by a chronic neurological disorder like Parkinson's disease and advance the understanding of the physiology of the disease. The authors discovered that the brain regions involved in the sense of touch and motor functions, whose functions are impaired by the disease, are the most prominent for differentiating between patients. In contrast, regions that support abstract thoughts are more typical of the healthy brain fingerprint. They also found that the more severe the motor symptoms, the more distinctive the patient's brain-fingerprint. However, they also report that in Parkinson's disease, brain activity tends to be more variable over short periods of times, which makes patients' brain-fingerprints more elusive to differentiate. Nevertheless, the study shows that the brain-fingerprint of patients is related to the cortical topography of the neurotransmitter systems affected by Parkinson's disease. Overall, this study demonstrates the potential of brain-fingerprinting as a tool to advance clinical neuroscience towards improved understanding and future interventions against neurological disorders.

Keywords:

Movement disorders, Parkinson's disease, neural oscillations, spectral parametrization, magnetoencephalography, brain fingerprinting.

Introduction

The neurophysiological origins of the characteristic, yet highly variable, motor and non-motor symptoms of Parkinson's disease (PD) are still debated [1–3]. The disease manifests a disparate range of structural, hemodynamic, and electrophysiological brain changes: from abnormal patterns of cortical thickness[4–7], to increased frequency-specific transients (beta band: 15 to 35 Hz)[8–10], and chronic slowing of brain activity[1,11,12]. Altered ongoing brain activity in PD also affects patients' brain-network characteristics (connectomes), which are related to the hallmarks of motor and cognitive impairments of the disease[13–16].

Recently, connectomes have been used to derive so-called *brain-fingerprints*, which enable the biometric differentiation of individuals based on their neuroimaging phenotypes[17–20]. Brain-fingerprinting posits that components of functional magnetic resonance imaging (fMRI) data or electrophysiological recordings of an individual remain relatively unchanged across data instances, and therefore are characteristic of the person[17,18,21]. When associated with behavioral and complex individual traits across large data repositories, the brain-fingerprinting approach promises to advance the understanding and characterization of the biological nature of personal health and disease trajectories[17,21–24].

In patients, however, there is early evidence that connectome brain-fingerprints tend to be more variable over time, such as in mental-health syndromes and related at-risk groups[25,27,28]. When the variability of brain-fingerprint features over time is high, the differentiation accuracy of the individual is low. In patients, such variability may confound which brain-fingerprint features differ between health and disease and limit the identification of how brain-fingerprint features are changed by treatment interventions.

In PD, the hemodynamic signals of fNIRS show increased temporal variability in patients with severe symptoms[29]. These temporal inconsistencies may also negatively affect the stability of individuals' connectome brain-fingerprints derived from fMRI. By extension, neurophysiological activity may also express greater temporal variability in patients with PD, especially in unimodal regions of the brain functional hierarchy where their coupling with hemodynamic signals is the strongest[30]. The individual differentiation of patients using connectome brain-fingerprints derived from neurophysiology is therefore expected to be particularly challenging, as previously observed with magnetoencephalography (MEG)[31] .

An additional issue to consider with connectome brain-fingerprints is that several types of brain connectomes can be derived from different derivatives of the neuroimaging or neurophysiological time series. This issue is particularly current with EEG and MEG[32]. It is therefore unclear whether the variability of connectome brain-fingerprints reported so far in PD research does originate from alterations of local brain activity caused by the disease, which would secondarily affect patients' connectomes. Moreover, electrophysiological brain activity

comprises both periodic and aperiodic signal components[33,34]. Indeed, little is known about the contribution of arhythmic/ aperiodic brain activity to the multi-spectral abnormalities reported in PD.

In a recent study involving healthy young adults, we demonstrated that frequency-specific measures of neurophysiological activity across the cortex from brief, task-free MEG data define *spectral* brain-fingerprints that remain specific of each individual over remarkably extended periods of time[21]. Here, we extend this spectral brain-fingerprinting approach to older healthy participants and patients with Parkinson's disease to ascertain their within and between-group inter-individual differentiability. Through this procedure, we sought to identify distinctive neurophysiological features of spectral brain-fingerprints in Parkinson's disease, and probe their possible association with clinical traits, functional brain organization[35], and cortical atlases of neurotransmitter systems that are relevant to the neuropathophysiology of the disease[36].

Results

We collected a minimum of 10 minutes of task-free MEG data from 79 patients with PD and 54 healthy age-matched controls (HC; demographic data in Table S1). We then source-imaged the MEG sensor data constrained to each individual's T1-weighted structural MRI[37]. We estimated the power spectral density (PSD) of the MEG source signals within each parcel of the Desikan-Killiany atlas[38] to derive the spectral brain-fingerprints of all participants[21] (see Methods).

Spectral brain-fingerprinting of patients with Parkinson's disease.

The brain-fingerprinting procedure consisted in assessing the similarity between the cortical spectral features derived from two approximatively 4-minute-long non-overlapping MEG recording segments from each participant, against the same features derived from the other participants[21]. The spectral features were determined across the [0, 150Hz] Hz frequency range (broadband spectral brain-fingerprint). We validated the approach by first extending our original fingerprinting results obtained with young-adult participants[3] to a group of older healthy individuals (age range: 40-78 years-old). We then proceeded to differentiate between patients with PD using spectral brain-fingerprinting (Figure 1). As a final challenge to the approach, we set to differentiate every patient with PD from healthy participants (i.e., patients vs controls). We computed bootstrapped confidence intervals (CI) around the differentiation accuracy scores obtained in these three brain-fingerprinting challenges (see Methods).

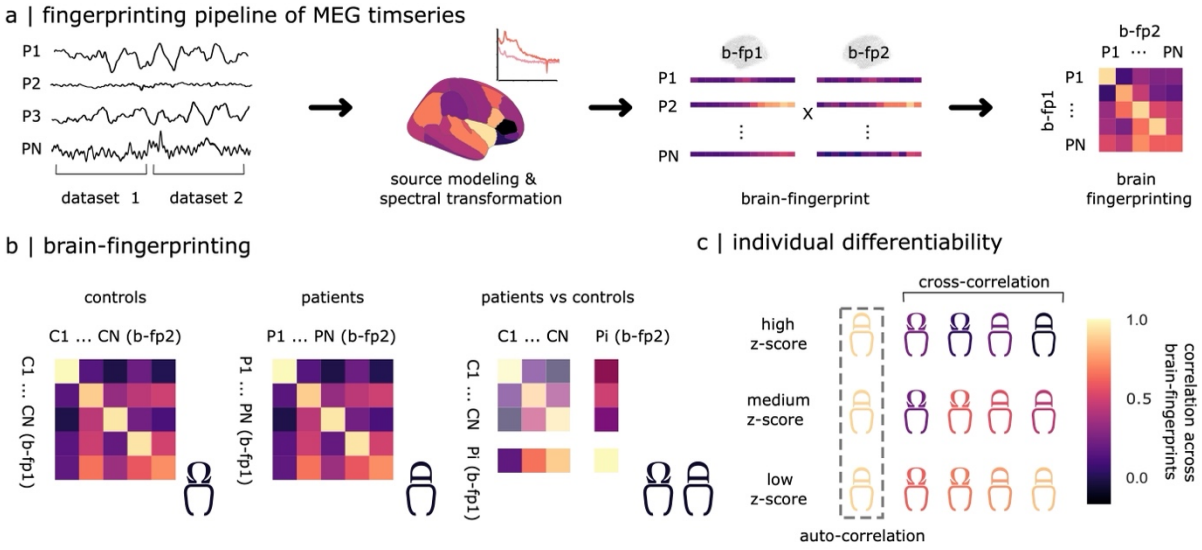

Figure 1: Spectral brain-fingerprinting pipeline and study design.

(a) The spectral power of MEG source time series is estimated from each parcel of the Desikan-Killiany atlas, from each data segment (dataset 1 and dataset 2) recorded from each participant (each approx. 4-min long). The resulting power spectra define the two spectral brain-fingerprints (b-fp1 and b-fp2) derived from each dataset[38]. A confusion matrix of the auto- and cross-correlation statistics of the spectral brain-fingerprints between participants determine their respective identifiability, as shown in (c). (b) We used the resulting spectral brain-fingerprints to differentiate i) between healthy controls, ii) between patients with PD, and iii) between each patient with PD against healthy controls. (c) We defined individual differentiability as the autocorrelation between the two spectral brain-fingerprints obtained from each participant, z-scored with respect to their cross-correlation with the spectral brain-fingerprints from the other study participants.

We found that the differentiation accuracy between older healthy participants (89.8%, [88.0, 94.0] CI; Figure 2a) is similar to the 96-% differentiation accuracy previously reported in younger health participants[21]. The differentiation between patients with PD is substantial, but less accurate than between age-matched controls (77.2%, [74.7, 81.7] CI). The differentiation of individual patients from healthy controls falls in a similar range of accuracy (81.1%, [81.0, 83.5] CI).

We then tested the respective relevance to PD neurophysiopathology of the rhythmic (band-limited, oscillatory) and arhythmic (broadband, scale-free 1/f) signal components of electrophysiological brain activity [33,34]. We parametrized the regional MEG-source power spectra into arhythmic and rhythmic components[33] and assessed individual differentiability from the resulting arhythmic brain-fingerprints.

We found that overall, the inter-individual differentiation performances using arhythmic brain-fingerprints were lower, but qualitatively similar to those from using the entire spectral brain-fingerprints: 74.1% (CI [72.0, 78.0]) between older healthy participants, 66.5% (CI [62.9, 71.4]) between patients with PD, and 71.5% (CI [69.6, 75.9]) between individual patients and age-matched healthy controls (see Figure S1 and Supplemental Information).

We repeated the same analyses using spectral brain-fingerprints defined only from the rhythmic components of neurophysiological power spectra, approximated as the residuals of the original spectral brain-fingerprints after their arhythmic components were removed (see Methods). We found that individual differentiation was more accurate with the rhythmic than with the arhythmic brain-fingerprints: 92.6% (CI [90.0, 96.0]) between older healthy participants, 86.7% (CI [82.9, 91.4]) between patients with PD, and 90.5% (CI [89.9, 92.4]) between individual patients and age-matched healthy controls (Figure S2).

We quantified the respective contributions of each cortical region to the spectral brain-fingerprints[18,40] by deriving intraclass correlation (ICC) scores. ICC scores enable the identification of the neurophysiological features that are the most consistent across individuals, between their respective spectral brain-fingerprints.

Frontal and medial cortical regions were the most salient features of the spectral brain-fingerprints of age-matched healthy participants (Figure S3a). In patients with PD, a set of cortical regions distributed bilaterally over the pre- and post-central gyri were the most prominent features of their spectral brain-fingerprints (Figure S3b-c and Figure 4b right panel).

Our previous work demonstrated that spectral brain-fingerprints that enable inter-individual differentiation of young adults can be derived from data lengths as short as 30 seconds[21]. We therefore tested the replicability of the approach with the present groups of older healthy participants and patients with PD (see Methods). We observed qualitatively similar performances in differentiation accuracy from these brief recordings that those from longer recordings (scatter plots in Figure 2a): 84.9% between healthy participants (computed 95% CI [83.1, 86.7]), 77.2% between patients with PD (95% CI [74.4, 79.9]) and 81.2% between individual patients and healthy controls (95% CI [78.7, 83.7]).

We propose that the differences in differentiation accuracy between groups can be visually appreciated using low-dimensional mapping of spectral brain-fingerprints with t-distributed stochastic neighbour embedding (t-SNE; see Figure 2b for a subset of 40 patient and control participants, and Figure S2 for all participants)[41]. The t-SNE qualitatively preserves the distances between data points in their native high-dimensional versions. We found that the 2-D Euclidian distances between each participant's two spectral brain-fingerprints scaled linearly with the differentiability of the individual (r=-0.55, t(131)=-7.46 p=1.05e-11; Figure 2c): the smaller the

distance between low-dimensional representations of the individual's spectral brain-fingerprints, the more differentiable they are.

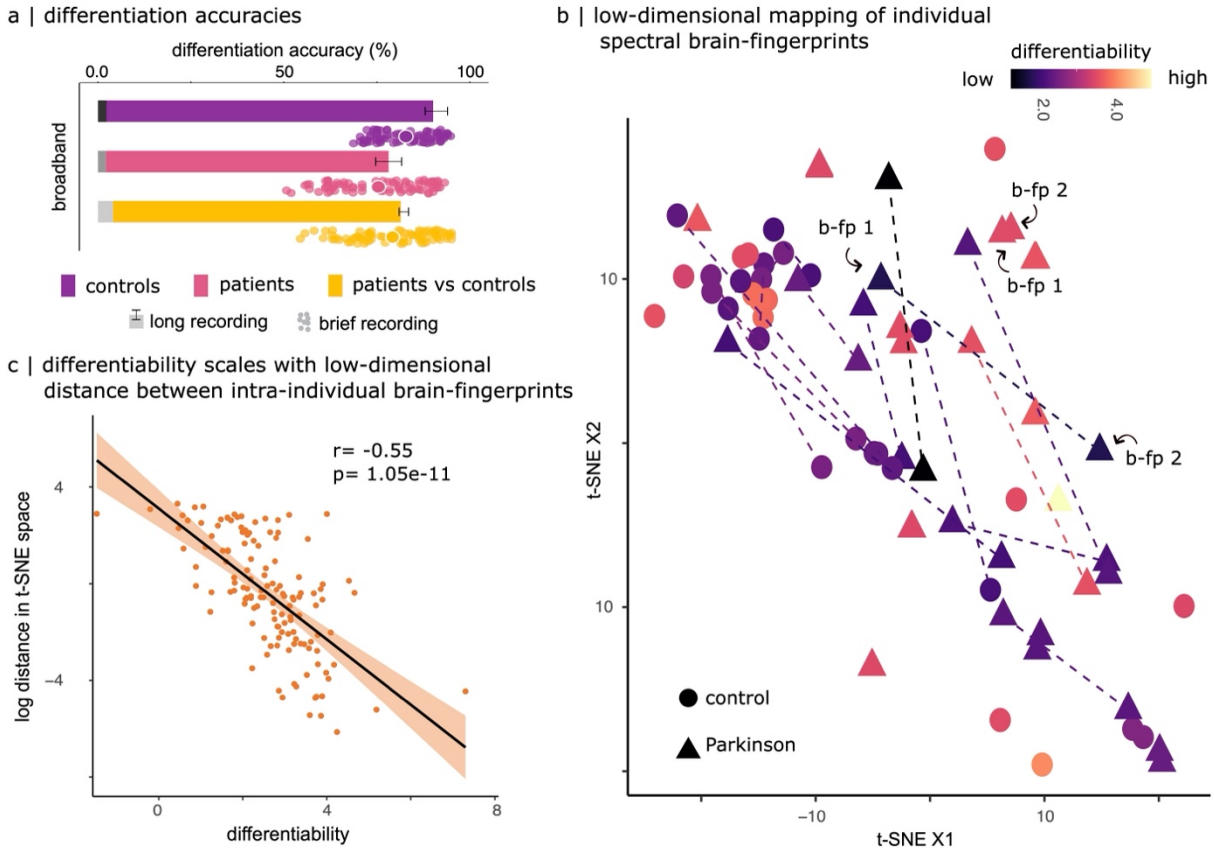

Figure 2: Individual differentiation of patients with Parkinson's disease and age-matched healthy controls.

(a) Differentiation accuracy using (broadband) spectral brain-fingerprints derived from 4-min data lengths (bar plots) and 30-sec data lengths (scatter plots). The scatter plots show the differentiation accuracy between all pairs of spectral brain-fingerprints derived from all 30-s segments extracted from the two original 4-min data segments. For control purposes, the grey segments at the foot of each bar plot indicate the differentiation accuracies from using empty-room MEG recordings around the participants' visits (see Methods). The error bars show bootstrapped 95% confidence intervals. (b) t-SNE mapping of individual spectral brain-fingerprints (sub-sample of 20 healthy controls and 20 patients with PD; see Figure S2 for display of all participants). Dotted lines connect between the two spectral brain-fingerprints derived from the two non-overlapping datasets used to produce the spectral brain-fingerprints of each participant. Note that dotted lines are not visible in participants with stable brain-fingerprints (plots overlap). (c) The (log-transformed) Euclidian distances between the two spectral brain-fingerprints of each individual in the t-SNE map scale linearly with their differentiability.

Individual differentiability scales with motor impairments.

We found that the individual differentiability of patients from their spectral brain-fingerprints was linearly related to the severity of their motor symptoms measured with the Unified Parkinson's Disease Rating Scale (UPDRS) part III (β=0.03, SE=0.01, 95% CI [0.01, 0.06], p=0.009, Bayes factor BF01=0.14; with nuisance covariates: participant age, education, disease duration, and head motion; Figure 3b and Table S2).

We then determined which brain regions contributed the most to this effect. To that end, we first derived reduced spectral brain-fingerprints by removing each cortical parcel in an iterative fashion (Figure 3c). We then evaluated the goodness of fit of the subsequent linear model of motor impairments scaling with individual differentiability from these reduced brain-fingerprints. We measured the contribution of the removed cortical region to the differentiability effect by measuring the resulting change in Akaike's information criterion (ΔAIC) between the original (Figure 3a) and reduced linear regression models (see Methods).

We found that only the left superior parietal cortex contributes to the association between individual differentiability and the severity of motor symptoms, based on a minimum absolute change of ΔAIC above 2[42].

Declining cognition in Parkinson's disease is associated with changes in brain structure and function [5,7,11,16]. We thus hypothesized that higher cognitive scores would moderate the association between the motor symptoms of patients with PD and their individual differentiability from spectral brain-fingerprints.

Our data do show an interaction between motor symptoms and cognition (β=0.05, SE=0.02, 95% CI [0.01, 0.10], p=0.025; after removal of age, education, disease duration, and head-motion nuisance effects; Figure 3b) in the linear regression model of individual differentiability, after the patient group was split based on MoCA scores (high vs. low MoCA; threshold 24; see Methods). Bayesian post-hoc analysis corroborated this finding (interaction effect: BF_{01}=0.28; see Supplemental Table S3).

We illustrate in Figure 3d this interaction between motor symptoms and cognition, with the power spectra extracted from the left superior parietal cortex, where the effect relating individual motor symptoms to the differentiability of brain-fingerprints is the most salient. The figure shows the respective regional spectra of low- and high-MOCA participants with lower and higher UPDRS III scores. Patients show increased spectral power in the lower frequency range (<10 Hz) with respect to healthy controls. The patients with lower motor and cognitive functions further show a marked decrease of faster brain activity (>15Hz; right panel Figure 3d).

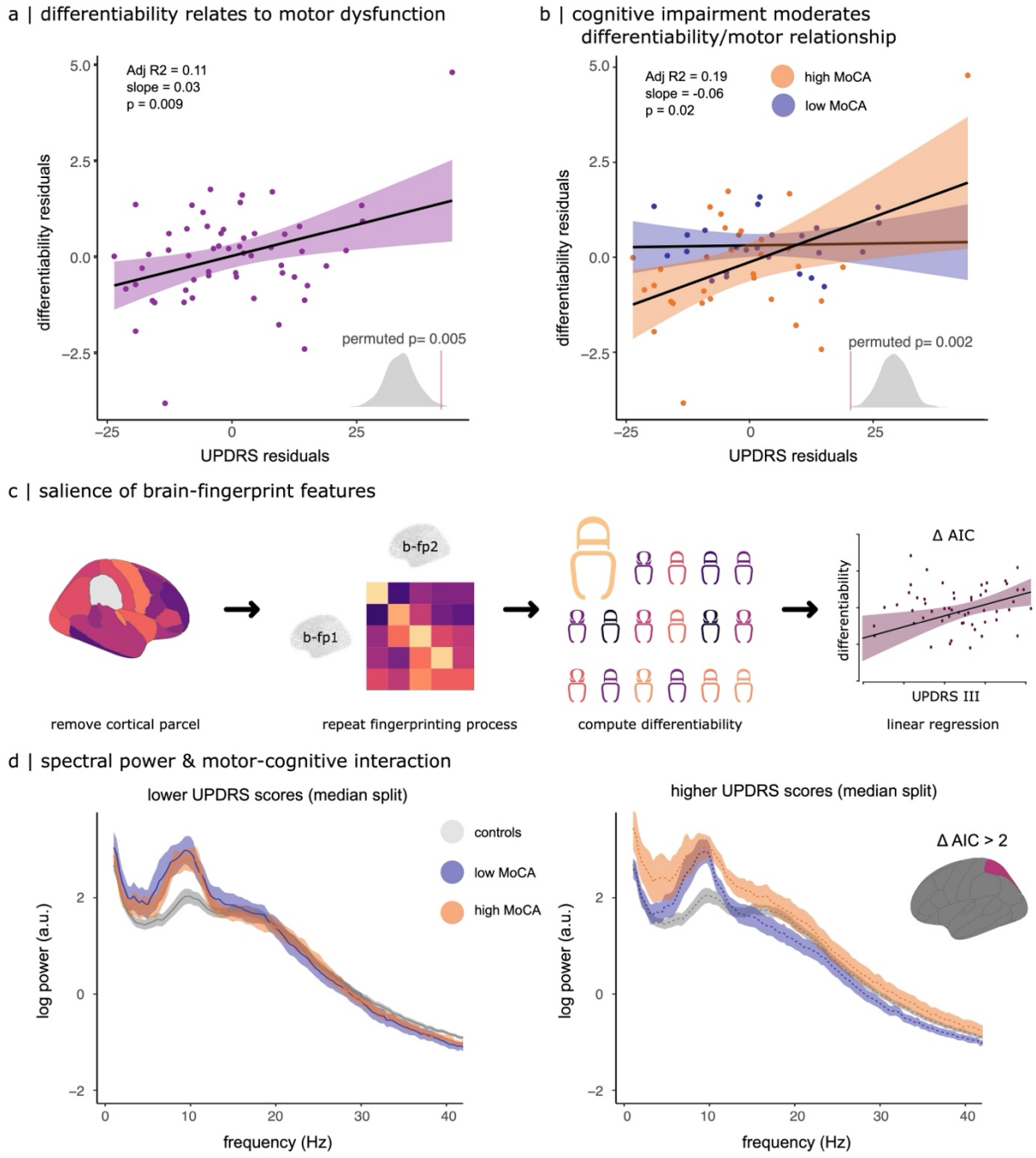

Figure 3: Individual differentiability and the impairment of motor and cognitive functions in PD. (a) The differentiability of patients from their brain-fingerprints relates to the severity of motor symptoms measured by the UPDRS part III scale. We obtained the histogram of regression coefficient (betas) under the null hypothesis of no group effect from n=1000 random permutations of individual differentiability scores (bottom right). (b) Cognitive impairment measured by MoCA scores interacts with motor symptoms in their association with the differentiability of patient brain-fingerprints. (c) The relative changes of Akaike's information

criterion (ΔAIC) determine which region(s) of the spectral brain-fingerprint contributes the most to the association between individual differentiability and PD motor symptoms. (d) Power spectra of neurophysiological signals in the left superior parietal cortex show the interaction between motor symptoms and cognitive functions. The data were derived from patients presenting high vs. low MoCA scores (different colors), and high vs. low UPDRS III scores (left vs. right graphs) using median splits of the cohort, for visualization. Shaded region depicts the standard error on the mean.

We verified that the individual differentiability of arhythmic brain-fingerprints remains associated with motor symptoms (β=0.02, SE=0.01, 95% CI [0.00, 0.04], p=0.03; BF_{01}=0.33; Supplementary Table 4 and Figure S7 & Figure S8). The salience analysis using the ΔAIC metric also confirmed that the left superior parietal cortex contributed the most to this association (Figure S7 & Figure S8). However, we did not find an interaction between motor and cognitive symptoms based only on arhythmic brain-fingerprints (β=0.02, SE=0.02, 95% CI [-0.02, 0.05], p=0.29; BF_{01}=1.20; Supplemental Table 5). In a similar fashion, there is no linear association between the individual differentiability of rhythmic brain-fingerprints and motor symptoms (β=0.03, SE=0.02, 95% CI [-0.00, 0.06], p=0.06; BF_{01}=0.49), with only limited evidence for a motor-cognitive interaction (β=0.06, SE=0.03, 95% CI [-0.00, 0.12], p=0.06; BF_{01}= 0.47; Supplemental Tables 6 and 7).

Decoding Parkinson's disease stages from spectral brain-fingerprints.

We tested whether spectral brain-fingerprints are related to the clinical stages of the disease. We designed binary classifiers to decode the disease stage of patients as "early" or "advanced" (as per their respective scores on the Hoehn & Yahr scale: HY< 2 or HY≥ 2, respectively)[43,44] from the spectral brain-fingerprint features at each cortical parcel (see Methods).

The resulting maps of regional decoding accuracy indicate that the decoding of the patients' clinical stage is driven the most by a broad set of cortical regions, with the best decoding performances obtained from the right post- and pre-central gyri (63.7% and 62.3% respectively; Figure 4a right panel). In later stages of the disease, faster brain activity (>15Hz) and slower activity ([6,9] Hz) are respectively suppressed and increased in these regions (Figure 4a left panel). We noted that the cortical topography of disease-stage decoding is similar to the cortical distribution of the most salient cortical regions of the spectral brain-fingerprints of patients (Figure 4b; r= 0.43, $p< 0.001$, $p_{spin}= 0$)—a robust finding regardless of the cross-validation method used for designing the binary classifiers (Figure S9). Note that reported effects (here and below) may be stronger than all observations from the spin tests from permuted data, yielding a null p_{spin} value.

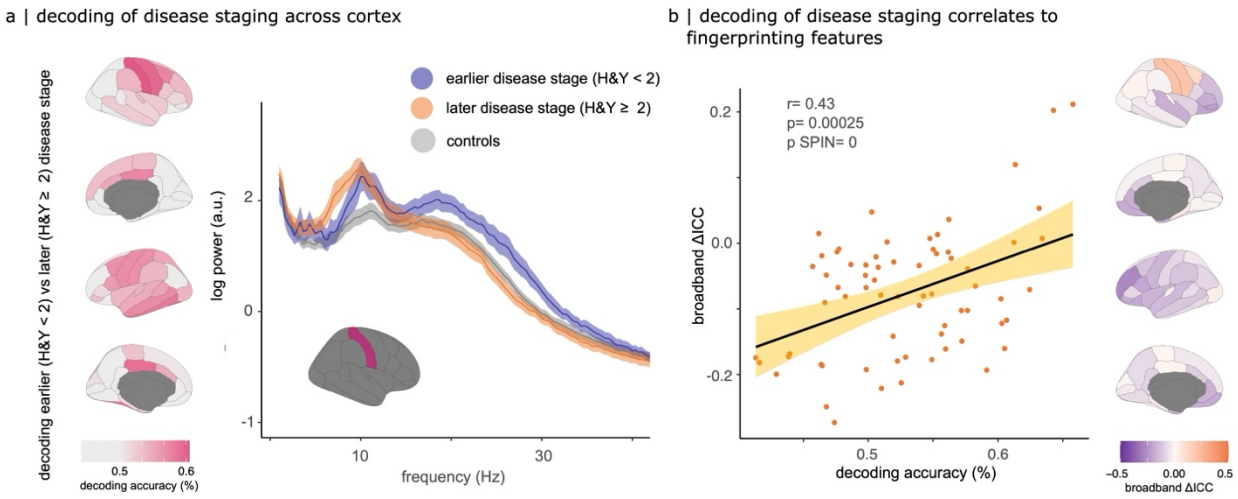

Figure 4: Decoding of Parkinson's disease stages from features of the spectral brain-fingerprints. (a) Left: topography of decoding accuracies of Parkinson's disease stages (binarized Hoehn & Yahr scores) from the spectral brain-fingerprint features of each cortical parcel. Right: power spectra of the neurophysiological resting-state signals generated in the right postcentral gyrus region, where decoding of Parkinson's disease stages is the most accurate. Shaded areas show the standard errors on the mean across the respective groups. (b) Left: scatter plot of the decoding accuracy of Parkinson's disease stages at each cortical parcel against the saliency of the brain-fingerprints of each cortical parcel (Δ ICC, right). Saliency of PD brain-fingerprints were obtained by subtracting the respective ICC topographies of between-patients and between-controls differentiations. Note that the resulting cortical map is similar to that of panel (a) because the ability to decode early vs. advanced Parkinson's disease stages from a cortical region is linearly associated with its saliency in the patient spectral brain-fingerprint.

Parkinson's disease alterations of brain-fingerprints align with the brain's functional hierarchy and the cortical topography of neurotransmitter systems.

We explored whether the topography of the most salient features of PD spectral brain-fingerprints (broadband Δ ICC; Figure 4b) is related to the hierarchical, unimodal-to-heteromodal gradient of functional brain organization[35] (see Methods). Our analysis confirmed the spatial similarity between the two cortical topographies (r=-0.51, t(66)=-4.79, $p< 0.0001$, p_{spin}=0; Figure 5a).

Transmodal regions colocalized with salient features of the spectral brain-fingerprints of older healthy adults. In contrast, the salient features of patients' spectral brain-fingerprints aligned with the unimodal, primary sensorimotor regions of the cortex functional hierarchy.

We also tested whether the most salient features of PD spectral brain-fingerprints were also topographically related to the cortical distribution of major neurotransmitter systems. We retrieved 19 normative cortical maps of 9 neurotransmitter systems from the *neuromaps* toolbox[36] (Figure 5b) and computed their spatial cross-correlation with the saliency map of PD

spectral brain-fingerprints (Figure 4b; see Methods). The cortical distributions of serotonin-4 (r=-0.38, p_{FDR}=0.006, p_{spin}=0.004), cannabinoid-1 (r= -0.49, p_{FDR}=0.00041, p_{spin}=0.00), and mu-opioid receptors (r=-0.40, p_{FDR}=0.0048, p_{spin}=0.005) are negatively correlated with the topography of PD spectral brain-fingerprints, and so is the cortical distribution of the norepinephrine transporter (r=0.43, p_{FDR}=0.0026, p_{spin}=0).

We noted that the cannabinoid, opioid, and serotonin systems are topographically concentrated in temporal and frontal regions, which matched the most salient spectral brain-fingerprint features of healthy controls (Figure 5b & Figure S3a). In contrast, the high concentration of norepinephrine transporters in the somato-motor cortices is aligned with the most salient spectral brain-fingerprint features of Parkinson's disease (Figure 5b & Figure S3b).

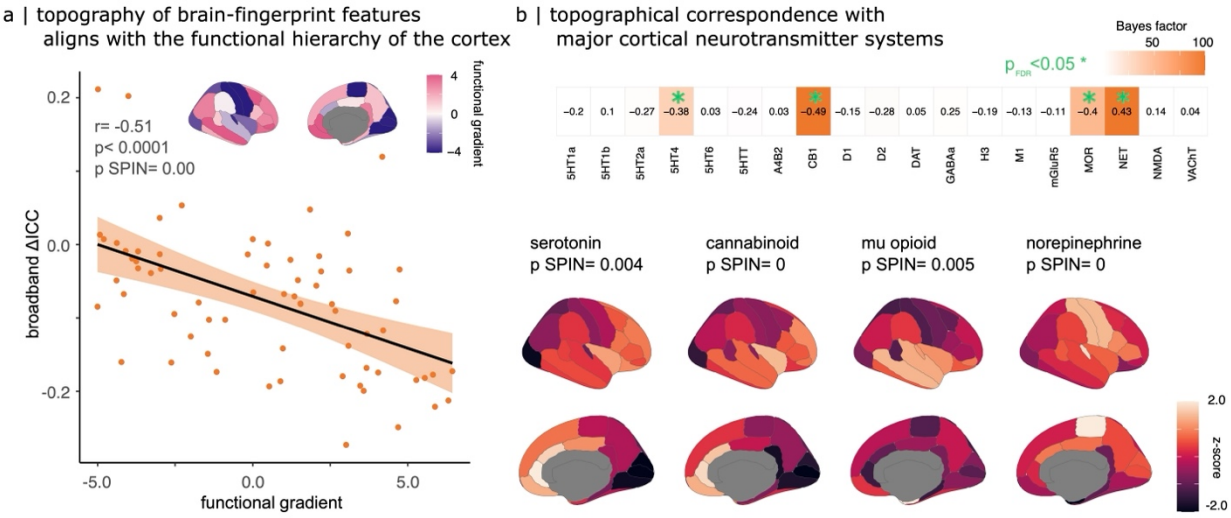

Figure 5: Topographical alignment between spectral brain-fingerprints, the functional hierarchy of cortex, and neurotransmitter systems.
(a) Top: The cortical topography of the first unimodal-transmodal functional gradient, retrieved from *neuromaps*[36]. Bottom: The respective weights of cortical regions in the functional gradient (*neuromaps* toolbox[36]) are linearly related to their saliency in the PD brain-fingerprint (Figure 4b right). (b) Top: Bayes factor analysis of the topographical alignment between PD brain-fingerprint features (Figure 4b) and the atlases of cortical neurochemical systems shows strong alignment of the serotonin, cannabinoid, mu-opioid, and norepinephrine systems. Bottom: selected neurochemical cortical atlases retrieved obtained from *neuromaps*[36].

Short-term moment-to-moment variability of spectral brain-fingerprints in Parkinson's disease.

Why are patients with PD differentiated with less accuracy than age-matched controls from their spectral brain-fingerprints? We tested how their two spectral brain fingerprints vary between datasets (autocorrelation) compared to how distinct they are from other participants (cross-correlation). We found that the cross-correlation of spectral brain-fingerprint features between

healthy participants, and between patients are similar within their respective groups (Figure 6a). However, the autocorrelation of spectral brain fingerprints is significantly reduced between datasets in patients (t=2.24, p=0.02; permutation t-tests). We conclude that the reduced individual differentiation accuracy of patients with PD is due to the greater short-term variability of their brain activity, tested here within 10 minutes of the same recording session.

To corroborate this point, we expanded the analysis of spectral brain-fingerprints derived from shorter (30-s) datasets. The premise was that if the short-term variability of patient brain activity is more pronounced, the accuracy of individual differentiation based on successive spectral brain-fingerprints would be expected to decrease with the gap duration between datasets, more rapidly in patients than in healthy controls.

Our findings corroborate this hypothesis: patient differentiation accuracy decreases more rapidly with the gap duration between successive spectral brain-fingerprints, compared to age-matched controls (β=-1.29, SE=0.55, 95% CI [-1.94, -0.65], p<0.001, BF_{01}=2.71 e-3; Table S8 and Figure 6b).

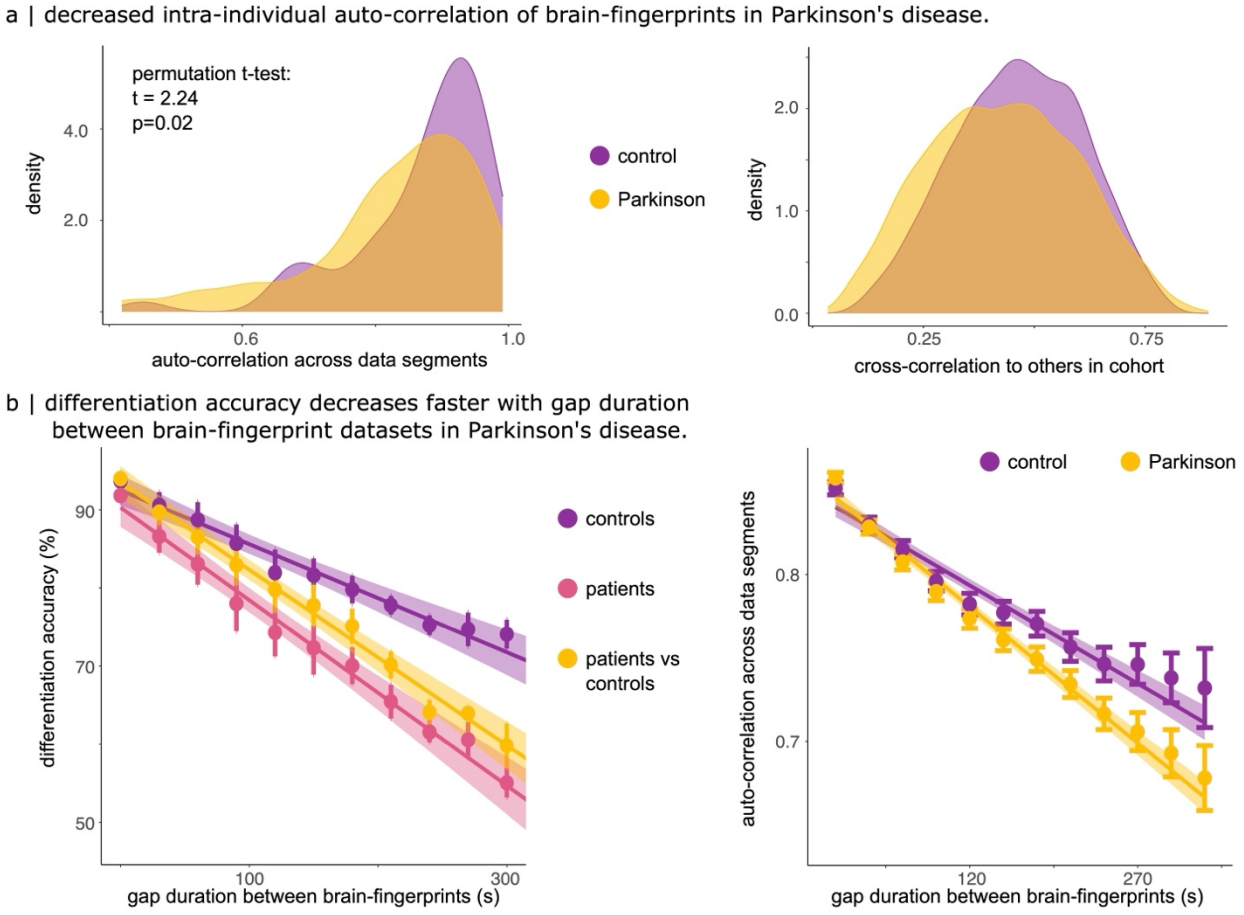

Figure 6: Pronounced short-term variability of spectral brain-fingerprints in Parkinson's disease. (a) Density plots of auto- (left) and cross-correlation (right) statistics between spectral brain-fingerprints within (autocorrelation) and between (cross-correlation) participants. Left: empirical density of autocorrelation statistics between two consecutive brain-fingerprints of participants in the control and PD cohorts. The wider distribution of the distribution of PD cohort autocorrelation statistics indicates that consecutive spectral brain-fingerprints are more variable in patients. Right: the empirical densities of inter-individual cross-correlation statistics of spectral brain-fingerprints are similar in the patient and control groups. (b) Individual differentiation from brief brain data segments (spectral brain-fingerprints derived from 30-s datasets). Left: The individual differentiation accuracy decreases with the gap duration between the datasets used to derive the spectral brain-fingerprints. The decrease is faster in patients, as expected from the lesser intra-individual autocorrelation of patient spectral brain-fingerprints shown in (a). This is also confirmed in the right panel, showing how the intra-individual autocorrelation between consecutive spectral brain-fingerprints decreases faster in patients than in healthy controls. Shaded regions depict the standard error on the mean.

Spectral brain-fingerprints are robust against data recording artefacts

We verified the robustness of spectral brain-fingerprints against environmental and physiological artifacts.

We found that individuals are not differentiable on the basis of environmental factors that would be specific of their respective days of recording, using the empty-room MEG recordings collected around each study visit. We pre-processed the empty-room recordings similarly to the participants data and mapped each session's empty-room data onto the respective participant's cortical surfaces, using the same imaging projectors as those for their original MEG data. The accuracy of empty-room individual differentiation was considerably lower the actual spectral brain-fingerprints (<5%; Figure 2a & Figure S4).

Second, we tested the robustness of brain-fingerprinting against typical physiological artifacts, including head motion, heart-rate variability, and eye blinks. The accuracy of brain-fingerprinting differentiability was correlated with head motion in the PD-cohort (r= 0.24, p= 0.04), but not with cardiac nor ocular artifacts (r= -0.04, p= 0.71; r= -0.08, p= 0.46 respectively; Figure S6). This effect was, however, relatively weak: a Bayesian post-hoc analysis indicated weak evidence for the alternative hypothesis (BF= 2.04). Nevertheless, we included head motion as a nuisance covariate in all regression analyses reported herein of the relationship between patient brain-fingerprint differentiability and symptoms (see Methods). We also note that healthy controls and patients showed no differences in terms of statistical measures of physiological artifacts (head motion: t(64.34)= 0.41, p= 0.68; EOG: t(123.88)= -0.91, p=0.36; ECG: t(64.41)= -1.24, p=0.22).

Previous literature has reported cortical thickness abnormalities in PD across the cortex[4–7]. We, therefore, tested whether changes in cortical thickness related to PD accounted, in part, for the fingerprinting performances. We estimated cortical thickness from the structural MRI data using

Freesurfer (*recon-all*) in both groups of participants with available MRIs (n=134; see Figure S5a). We then used the healthy controls cortical thickness measures to standardize the patient's cortical thickness maps via a z-score transform. There was no significant linear association between individual differentiability and the average standardized cortical thickness of patients with PD (b= -0.03, SE= 0.07, 95% CI [-0.16, 0.11], *p*= 0.69; Figure S5b). Moreover, the topography of the most salient regions for PD brain-fingerprinting were not related to the topography of standardized cortical thickness of patients with PD (Pearson correlation: r=0.11, t(66)=0.88, *p=0.38)*. We conclude that the individual differentiability of patients with PD from their spectral brain-fingerprints was not influenced by structural cortical alterations caused by the disease.

Discussion

Brain fingerprinting identifies individually differentiable patterns of brain activity that may also be associated with individual complex traits[17,18,21,45]. Here we demonstrate the relevance of the approach to the clinical neuroscience of Parkinson's disease. We derived brain-fingerprints from short segments of ongoing neurophysiological (MEG) brain activity, recorded in task-free conditions. Our data show that patients with PD can be individually differentiated from each other and from other healthy individuals, from the spatial distribution of the spectral properties of their neurophysiological signals on the cortex. We further demonstrate that the individual differentiability of patients with PD scales with the severity of their motor and cognitive symptoms.

Patients can be differentiated from healthy controls with 81% accuracy. Our data also show, however, that the differentiation between patients with PD is on average 15% less accurate than between age-matched healthy controls (Figure 2a) but remains considerably higher than from environmental noise on the day of the participants' visits (Figure S4).

Brain-fingerprints of the symptoms of Parkinson's disease.

We used a measure of differentiability between successive brain-fingerprints to differentiate between individuals in the tested cohorts. We found that differentiability relates to both motor and cognitive symptoms across patients with PD (Figures 3). Patients who were more differentiable from the cohort were also afflicted with more severe motor symptoms. This effect was mediated by preserved cognitive abilities, whereby patients with higher general cognitive scores showed a stronger relationship between their motor symptoms and the differentiability of their brain-fingerprint.

Patients demonstrating cognitive decline may show greater moment-to-moment variability of their brain-fingerprint, thereby attenuating the relationship between motor dysfunctions and individual differentiability. Prior research has established the variability of behavioural assessments to the severity of cognitive symptoms in PD[46–48]. Recent PD research work further demonstrates a relationship between behavioural variability and abnormalities in cortical thickness in the temporal and parietal cortex[49]. While there is scant evidence linking behavioural

and neurophysiological variability in PD, previous fMRI studies have reported an association between the variability of brain activity across the lifespan and cognitive performance[50–52]. For these reasons, we can speculate that a declining cognition may induce greater variability of behavioural markers and of brain-fingerprints.

In a similar vein, the aging research literature suggests that decreases in dopaminergic activity augments neural noise, with subsequent decreases in cognitive performances, increased behavioural variability and confusion between cortical representations[53,54]. Our results are aligned with these constructs and may inspire more research to specifically bridge between moment-to-moment variability of behaviour and the temporal variability of brain-fingerprints in Parkinson's disease.

Neurophysiological alterations of the brain-fingerprint in Parkinson's disease.

Previous studies of the neurophysiology of PD have reported alterations in frequency-specific signalling of motor and subcortical structures associated with motor symptoms[55,56]. Our results indicate that patients with PD can be individually differentiated, and their respective clinical features identified, from neurophysiological brain-fingerprint features across the cortex and across the neurophysiological frequency spectrum.

Although neurophysiological activity in the pre and post central gyri was the most prominent fingerprint features in patients, the spectral features of the left superior parietal cortex showed the strongest association between patient differentiability and symptoms. Previous anatomical studies suggest that the superior parietal lobule and premotor/somatomotor regions are strongly inter-connected with one another[57,58]. Evidence from lesion studies also suggests that damage to the left superior parietal cortex impacts a variety of skills including visuo-spatial, working memory, cognitive, and motor functions[57,59–62]. Indeed, the left superior parietal cortex plays a role in sensory-motor integration of information[63,64] for working memory[65,66]. These aspects support our observation that this region help differentiate between patients with PD, in accordance with their motor and cognitive symptoms. The biological (e.g., microstructural, genetic) underpinnings of neural signalling and their associations with PD motor and cognitive symptoms have yet to be explored.

The regions that enable decoding of disease staging from neurophysiological signals colocalize with the topographical features of the PD brain-fingerprint. The pre and post central gyrus are the regions with the highest decoding accuracy of disease stages are also those that significantly contribute to the differentiation between patients (Figure 4a). This result held regardless of the strategy used to train the classifier (Figure S9). Further studies of the alterations of the spectral brain-fingerprint associated Parkinson's disease will help bridge between the clinical presentation of the disease to its neuropathological mechanisms.

Recent studies have shown alterations of arhythmic brain activity in PD patients[12,67,68]. Here we show that the arhythmic component of the neurophysiological spectrum can differentiate between individuals and contributes to the association between inter-individual differentiability and motor symptoms. However, the contribution of arhythmic activity to the motor-cognitive interaction is more tenuous than when considering the entire neurophysiological spectrum, which emphasizes the role of its rhythmic components in the characterization of the disease manifestations.

Parkinson's disease alters large-scale neurophysiological signaling asymmetrically across the cortex

We found that the most salient brain-fingerprint features for differentiating between patients with PD reside in the primary sensorimotor cortex (Figure 4b right panel & Figure S3c). This finding resonates with the wealth of literature that reports alterations of brain activity in sensorimotor regions in Parkinson's disease[10,69,70]. Our results indicate that these functional aberrations may represent stable markers that are characteristic of individuals with PD and contribute to characterizing the neurophysiological signature of each patient's case. We anticipate that these individual feature alterations in Parkinson's disease become useful brain-signal signatures of the patient's clinical presentation.

Brain-fingerprint features in regional components of the default-mode network (DMN) were most prominent in healthy participants (Figure 5a & Figure S3a). Previous work has reported functional decoupling of the DMN in PD during rest and tasks[71–74]. These abnormal manifestations of the DMN have been related to the dopaminergic system, as they can be normalized with levodopa treatment [75,76]. Levodopa and dopamine agonists may therefore help normalize brain activity in DMN regions and consequently, contribute to standardizing neurophysiological signaling across patients. This may explain why the DMN regions, which sit higher in the brain functional hierarchy, contribute less to the individual differentiation between patients with PD (Figure 5a).

Possible neurochemical foundations of the brain-fingerprint of Parkinson's disease.

Our data suggest that monoamine neurotransmitters are associated with the brain-fingerprint of PD (Figure 5b). In particular, we found that the cortical topography of serotonin-4 receptor density is associated with the reduced neurophysiological stability of the PD brain-fingerprint, with an opposite association with norepinephrine. This means that the most salient anatomical features of the PD brain-fingerprint co-localize with lower concentrations of serotonin-4 receptors and higher concentrations of norepinephrine transporters. This observation aligns with previous report of degraded monoamines, and in particular dopamine, serotonin, and norepinephrine, in PD[77]. We note that we did not observe an association between features of the PD brain-fingerprint and dopamine concentrations, probably because the *neuromaps* data and our MEG analyses are both presently restricted to the cortical surface, while changes in dopaminergic signaling caused by PD primarily affect subcortical structures[78].

We also found that the cortical topography of the cannabinoid receptor-1 (CB1) system is also negatively association with the topographical features of the PD brain-fingerprint (Figure 5b). Prior work has documented an elevated concentration of CB1 receptors in the striatum, and suggests that this receptor system may play a role in the long-term depression of synapses for motor learning[61]. This has revealed CB1 as a potential therapeutic target in PD[81]. Our present results also highlight the potential participation of the cannabinoid system in the neuropathophysiology of PD and encourage more research in this area.

Taken together, we hope the present body of results inspires and serves continued efforts to define potential targets, and novel biomarkers for future treatments of Parkinson's disease.

Short-term variations of brain activity are more pronounced in Parkinson's disease.

We found that the brain-fingerprints of patients with PD are more variable over relatively short periods of time than those of age-matched healthy controls, which explained the slightly lower inter-individual differentiation accuracy observed in the patient group (Figure 6).

This greater, moment-to-moment variability of brain activity was expected from previous observations of pronounced sequent variability of fMRI connectomes in individuals with or at risk of mental health disorders[27], such as schizophrenia[28], and in the brain-network fingerprints of patients with PD[31] . Our data extend these observations to spectral derivatives of electrophysiological brain activity. These findings also align with reports of greater intra-individual variability of patient performances on cognitive tasks in PD[46,47,82].

Implications for personalized medicine.

Whether the brain-fingerprinting approach has potential for future clinical impact depends on its ability to stratify patients, identify novel disease features, and/or guide new treatment options.

Here we show that brief, as short as 30-second brain recordings differentiate between individuals[21]. These results are in line with previous published observations that the estimation of the spectral contents of resting-state brain activity stabilizes within 30s to 120s of MEG recordings[83]. We believe this is a strong asset of the MEG brain-fingerprinting approach for potential clinical adoption in patient populations, over fMRI and EEG alternatives.

Our data emphasize the increased variability of brain activity features in neurological and mental health disorders[25,27,28,84]. We foresee that patient trajectories may be delineated via future explicit measures of such variability of the brain-fingerprints features highlighted in the present study (see, e.g., Figure 6b). We also emphasize that the increased intra-individual variability of brain activity features in disease needs to be considered as a challenging, confounding factor in the design of emerging statistical and machine learning models to ensure their ability to generalize their patient stratification performances at scale.

To conclude, this study brings evidence for the clinical relevance of brain-fingerprinting based on the fast dynamics of neurophysiological brain activity. This approach captures meaningful clinical aspects of Parkinson's disease, and highlights candidate brain regions where the moment-to-moment stability of neurophysiological activity is altered by disease mechanisms. We anticipate that the data presented will pave the way for future research and discoveries in population neuroscience and personalized medicine of Parkinson's disease and other neurodegenerative disorders.

Methods

Participants. Data from healthy controls and patients with mild to moderate idiopathic PD were aggregated from several sources (40-82 years-old): data from 79 PD patients with extensive clinical, neurophysiological, and biological profiling were collected from the Quebec Parkinson Network (QPN; https://rpq-qpn.ca/[85]) initiative. All patients enrolled in the QPN study were prescribed a stable dosage of antiparkinsonian medication and showed a satisfactory clinical response. PD patients were instructed to take their medication as prescribed prior to any data collection. We included data from all QPN participants with complete and usable MEG, clinical, and demographic data. A sample of demographically matched healthy participants was also included from the PREVENT-AD (N=50)[86] and OMEGA (N=4)[22] repositories. All participants had undergone resting-state eyes-open MEG recordings using a 275-channel whole-head CTF system (Port Coquitlam, British Columbia, Canada) at a sampling rate of 2400 Hz (600-Hz antialiasing filter), with third-order gradient filters applied. All recordings were conducted at the same site and lasted at least 10 minutes.

MEG data preprocessing. MEG data were preprocessed using Brainstorm[87]; March 2021 distribution, running MATLAB 2019b (Mathworks, Inc., Massachusetts, USA) following good-practice guidelines[88]. The preprocessing pipeline followed previous published work performed on these data[89]. MEG sensor signals were bandpass filtered between 1–200 Hz to reduce slow-wave drift and high-frequency noise. Line noise artifacts (60 Hz) along with harmonics were removed using a notch filter bank. We derived Signal-Space Projectors (SSPs) to remove cardiac and ocular artifacts based on electro-cardiogram and electro-oculogram recordings, using an automated procedure in *Brainstorm*[87]. The MEG recordings were then epoched into 6-s non-overlapping segments and down-sampled to 600 Hz. Artifactual data segments with peak-to-peak signal amplitude or maximum signal gradient exceeding ± 3 median absolute deviations from the median across all epochs were excluded.

MEG source mapping. Brain source models were then derived from the individual T1-weighted MRI data available for each participant. The MRI volumes were automatically segmented and labeled using Freesurfer[90]. MEG was coregistered to the segmented MRI data using approximately 100 head points digitized on the day of the MEG session. Fourteen patients with

PD and 3 controls did not have useable MRI data—we consequently registered each of these participants to quasi-individualized anatomy created by warping the default Freesurfer anatomy to the available head digitation points and anatomical landmarks[90]. We produced MEG biophysical head models for each participant using the *Brainstorm* overlapping-spheres model (default parameters) applied to 15,000 elementary dipole sources constrained to the cortical surface (free orientation). Source maps for each participant and 6-s epoch were computed using dynamic statistical parametric mapping (dSPM; default parameters). The same processing pipeline was applied to two-minute empty-room recordings collected for statistical modeling of environmental noise around each participant's visit. Individual source time series at each cortical location was obtained from the first principal component of the three elementary time courses of each triplet of elementary sources at each cortical vertex. The resulting 15,000 time series were then clustered according to Desikan-Killiany cortical parcellation into 68 regions of interest[38] (ROIs), with one representative time series per parcel obtained from the first principal component of all source signals within each ROI.

Derivation of the spectral brain-fingerprints. Brain-fingerprints were then derived from the power spectrum of these ROI source timeseries. Power spectrum density (PSD) at each parcel was obtained with the Welch's method (time window of 3 s, 50% overlap). The resulting frequency range of PSDs was 0–150 Hz, with a frequency resolution of 1/3 Hz. Each individual's spectral brain-fingerprint consisted of the PSDs of all 68 cortical parcels, averaged across multiple 6-s epochs. As reported in Results, we derived two spectral brain-fingerprints from epochs corresponding to either the first or second half of the entire MEG session. We also derived spectral brain-fingerprints from shorter datasets of 30-s non-overlapping segments. In total, the number of features in each spectral brain-fingerprint was 68x451. The rest of the analyses were performed using in-house code in Python (3.7.6) and R (V 4.2.1).

Individual differentiation from spectral brain-fingerprints. We replicated the previously published fingerprinting approach based on the correlational differentiability of participants between data segments (Figure 1a-b)[21]. For each participant, we first compute all Pearson correlation coefficients between the first spectral brain-fingerprint of the participant and the second brain-fingerprint of all individuals in the same cohort, including the probe participant. Fingerprinting then consists of a simple lookup procedure along the row (or columns) of the (symmetrical) interindividual correlation matrix. The entry of the largest correlation coefficient indicates the match with the probe participant. This approach is repeated for all participants in the cohort, yielding a confusion matrix across all participants in the cohort based on the two instances of their respective brain-fingerprints. We defined the percent ratio of correctly differentiated individuals as the differentiation accuracy of the brain-fingerprinting procedure.

In the present study, we considered three types of differentiation challenges: i) between healthy participants, ii) between patients with Parkinson's disease, and iii) between each patient with PD against all healthy controls (i.e., patients vs controls; see Figure 1c). The purpose of the brain-fingerprint differentiation between healthy participants was to replicate our previous study with

younger adults[21] with a group of older participants and provided a benchmark differentiation accuracy for the age group of patient participants.

In this framework, individual differentiability measures how a participant can be distinguished from other individuals in the cohort based on their brain-fingerprint. We defined this measure as the z-scored Pearson correlation between the two brain-fingerprints of a given participant, relative to the mean and standard deviation across the correlations between this participant first brain-fingerprint and all other participants' second brain-fingerprints.

Bootstrapping of differentiation accuracy scores. We used bootstrapping to derive confidence intervals around the average differentiation accuracy scores obtained from the above procedure across the tested cohorts. We randomly selected a sub-sample of participants representing 90% of the tested cohort and performed brain-fingerprinting of their data to derive a differentiation accuracy score from that sub-sample. This process was repeated 1000 times, from different random subsamples of participants in the tested cohort. A 95-% confidence interval was derived from the 2.5th and 97.5th percentiles of the resulting empirical distribution of differentiation accuracies.

t-SNE visualization. We used the distributed Stochastic Neighbour Embedding (t-SNE) method as implemented in R (package M3C[41]) to project the two high-dimensional brain-fingerprints of each individual in a two-dimensional plane. The resulting plot across all participants is shown Figure S2; a subset of 20 individuals presenting the highest and lowest individual differentiability scores is shown Figure 2. From these 2-D maps, we estimated the correlation between the log-transformed Euclidian distance between each participant's brain-fingerprints and their respective individual differentiability scores. We performed an independent-sample t-test to determine if whether these distances are less in healthy controls than in patients with PD. We used *ggplot* with custom R scripts to produce these plots. All brain maps shown in Figure 3, 4 & 5 and in Supplemental Information were generated using R (V 4.1.2; with the *ggseg* package). The shaded areas shown in Figure 2c, 3a, 3b, 4b, 5a, & 6b represent the 95-% confidence intervals obtained from *stat_smooth*, also in R.

Ruling out possible biophysical and environmental artifacts. We investigated whether environmental noise and biophysical recording artifacts might have affected differentiation of individual participants. We related individual differentiability scores to the respective root-mean-squares (RMS) of measured ocular, cardiac, and head movement signals collected simultaneously with MEG (ECG, HEOG, VEOG, head-coils triplet channels, respectively). We derived the correlation of the three measures obtained with the individual differentiability of each participant from the entire cohort. The head motion RMS measure was also included as a nuisance covariate in the regression model linking individual differentiability and motor symptoms.

We also tested if environmental and instrument noise, which can vary from day to day, may have biased individual differentiation. We used the empty-room recordings collected around each

MEG session, to derive pseudo brain-fingerprints for each participant based on the cortical source maps of the noise recordings. We then estimated the differentiation accuracies obtained from these pseudo brain fingerprints, replicating our previously published approach[21].

Arhythmic/rhythmic spectral parametrization. We estimated how arhythmic and rhythmic spectral components of the brain-fingerprint contributed to individual differentiation. We first used *specparam* as available in *Brainstorm* to identify the best-fitting arhythmic components of the spectral features of each individual's brain-fingerprint in the 2-40 Hz range. Parameters for *specparam* were set to: peak width limits: [0.5 - 12 Hz]; maximum number of peaks: 3; minimum peak amplitude: 3 a.u.; peak threshold: 2 standard deviations; proximity threshold: 2 standard deviations; aperiodic mode: fixed. We used the resulting arhythmic models to derive brain-fingerprints based only on these features. Symmetrically, we then removed these arhythmic components from the original brain-fingerprints to assess how the rhythmic residuals of the brain-fingerprint contributed to inter-individual differentiation.

Saliency of brain-fingerprint features. We calculated intraclass correlations (ICC) to quantify the contribution of each cortical region towards differentiating between individuals. ICC quantifies the agreement between two measures, whereby here, the higher the ICC of a given brain-fingerprint feature, the more consistent it is across the two brain-fingerprints of each individual. The ΔICC maps depicted in Figure 4b and Figure S3 were obtained by first averaging ΔICC values within each of the canonical frequency bands and then across bands. Specifically, we averaged ΔICC within the delta 1–4 Hz, theta 4–8 Hz, alpha 8–13 Hz, beta 13–30 Hz, gamma 30–50 Hz, and high-gamma 50–150 Hz ranges to obtain six ΔICC maps, one per frequency band, and then averaged across all bands. The rationale is to weigh each frequency band equally in the derivation of the broadband ΔICC, regardless of their respective widths (e.g., the delta bandwidth is 4Hz; the high-gamma's is 100 Hz).

Neuroanatomy. We verified that neuroanatomical features, including changes caused by Parkinson's disease, did not confound the ability to differentiate participants based on their spectral brain-fingerprints. We measured z-scored deviations of cortical thickness (from *FreeSurfer*) for each cortical parcel and for each patient with PD, with respect to the mean and standard deviation observed across the age-matched healthy controls. We then fit linear regression models to test if: i) the most differentiable patients also showed greater deviations in cortical thickness, and ii) deviations in regional cortical thickness was related to regional ΔICC (Figure 4b right panel).

Individual differentiability and clinical scores. We tested whether the ability to differentiate an individual based on their brain-fingerprints was related to their clinical scored evaluation. We used the Unified Parkinson's Disease Rating Scale (UPDRS) part III[91] and the Montreal Cognitive Assessment[92] (MoCA) as scoring systems for motor and cognitive functions, respectively.

The UPDRS measures several facets of Parkinson's disease symptomology, including both motor and non-motor symptoms. We used the motor symptom subscale (UPDRS part III)[91], with the hypothesis that patients with more severe motor symptoms would also be more differentiable. We fit linear regression models in R (V 4.1.2) using the built-in *lm()* function to predict differentiability, including age, education, and disease duration as nuisance covariates.

$$differentiability \sim age + education + diease\ duration + head\ motion + UPDRS\ III$$

We hypothesized that individual differentiability would also be predicted by the severity of cognitive symptoms. We used MoCA scores as measures of participant's general cognitive function. We categorized patients using a "low" vs. "high" MoCA scores based on a common clinical cut-off, such that patients with a MoCA score above (respectively below) 24 were rated as cognitively healthy (respectively impaired)[92]. We fit a linear regression model using all the above-mentioned predictors, and the MoCA, and the interaction between MoCA and motor symptoms.

$$differentiability \sim age + education + disease\ \ duration + head\ motion + UPDRS\ III + MoCa + UPDRS\ III * MoCa$$

We used the *Bayesfactor* package in R to obtain Bayes factors (BFs) weighing evidence of the null hypothesis (excluding a predictor) against the alternative hypothesis (including the predictor of interest, i.e., UPDRS and UPDRS*MoCA). BF< 1 indicates that evidence favours the alternative hypothesis of an effect of the predictor.

We used Cook's distance (outlier threshold > 1) and the *check_model* function from the performance package in R to identify outliers and check model assumptions, respectively[93,94].

We ran non-parametric permutations to compute a p-value for each of the tested symptom-differentiability relationships. We permuted the association of patients' differentiability scores to their symptoms (i.e., permuted the rows of the differentiability vector), re-ran the above regression analysis and registered the value of the corresponding beta coefficient. From the empirical distribution of these beta values, we obtained a non-parametric p-value for the UPDRS III effect and the MoCA*UPDRS III interaction.

Relative contribution of frequency bands and ROIs for the differentiability relationships to clinical features. We quantified the importance of a ROI for the differentiability relationships to clinical features (i.e., UPDRS and MoCA) using an adapted leave-one-out approach. Here, we iteratively left out each feature of interest, recomputed differentiability with this feature removed, and re-fit the regression model using these values. For example, to calculate how important the delta band is in a given relationship, we computed differentiability using spectral data from all frequencies except for the delta band. We then fit a linear regression model using these "delta-left-out" differentiability scores and compared the change in AIC (ΔAIC) between this model and the full model (i.e., using all the frequency bands), with higher ΔAIC values indicating a more substantial contribution to the overall effect. We repeated these steps for

every frequency band of interest and ROI, iteratively computing differentiability, fitting a linear regression model, and computing the ΔAIC. To determine which ROIs contributed meaningfully to the differentiability relationships, we used a standard criterion of ΔAIC > 2 as our threshold.

Decoding disease staging from brain-fingerprints. We used the individual Hoehn & Yahr scores as indicators of individual disease staging in patients[43,44]. Here too, we binarized the scores around a value of 2 to stratify patients into two groups. This division distinguishes between patients with and without presentations of bilateral symptoms. We trained a linear support vector machine (SVM) classifier in R with default parameters, to identify each patient's disease stage category from their respective spectral brain-fingerprint features.

We ran SVM classification for each cortical parcel separately: data from a random sample of 80% of the patients was used to train the SVM classifier, which was subsequently tested on the remaining 20% of patients. We recorded the percent of held-out patients for whom the classifier correctly identified their Hoehn & Yahr category. We iterated this process 1000 times per cortical parcel to generate an empirical distribution of disease stage classification accuracy across the cortex.

We then estimated the spatial correlation between the cortical topographies of disease stage decoding accuracy and the regional ΔICC values of the brain-fingerprints (see **Saliency of brain-fingerprint features**). More specifically, we subtracted ICC values from the PD-cohort fingerprinting challenge and control-cohort challenge and correlated these differences in ICC across cortical ROIs to the decoding accuracies obtained from the decoding of Hoehn & Yahr scores.

Correspondence of brain-fingerprint features with the functional hierarchy of the cortex. We aimed to determine if the brain-fingerprints of individuals with Parkinson's Disease colocalized with the cortical topography of functional hierarchies[35].

We computed the Pearson's spatial correlation of ΔICC brain-fingerprint topography with the atlas map of the first gradient of the cortical functional hierarchy[35] available from *neuromaps*[36] and parcellated in the 68 regions of the Desikan-Killiany atlas[38]. We computed the related Bayes factors using the *correlationBF* function in R. We also estimated associated p-values using permutation tests controlling for the spatial autocorrelation of the data[96,97].

Correspondence of brain-fingerprint features with cortical neurotransmitter systems. Using a similar approach as in the above subsection, we estimated the Pearson's spatial correlation between the regional ΔICC values of the brain-fingerprints and each of the normative atlas maps (from *neuromaps*[36]) of 19 receptors and transporters from 9 neurotransmitter systems. These latter consisted of: dopamine (D1: 13 adults, [11C]SCH23390 PET; D2: 92, [11C]FLB-457, DAT: 174, [123I]-FP-CIT), serotonin (5-HT1a: 36, [11C]WAY-100635; 5-HT1b: 88, [11C]P943; 5-HT2a: 29, [11C]Cimbi-36; 5-HT4: 59, [11C]SB207145; 5-HT6: 30, [11C]GSK215083; 5-HTT: 100, [11C]DASB), acetylcholine (α4β2: 30, [18F]flubatine; M1: 24, [11C]LSN3172176; VAChT: 30,

[18F]FEOBV), GABA (GABAa: 16, [11C]flumazenil), glutamate (NMDA: 29, [18F]GE-179; mGluR5: 123, [11C]ABP688), norepinephrine (NET: 77, [11C]MRB), histamine (H3: 8, [11 C]GSK189254), cannabinoid (CB1: 77, [11 C]OMAR), and opioid (MOR: 204, [11 C]carfentanil).
Each map was parcellated using the 68 regions of the Desikan-Killiany atlas[38]. Statistical significance was determined after correction for multiple comparisons using a False Discovery Rate (FDR) as implemented in the R function *p.*adjust[98]. We derived Bayes factors to quantify the evidence in favour of the alternative hypothesis (i.e., a spatial correlation does exist) using the *correlationBF* function in R. For each significant spatial correspondence observed, we also estimated p-values based on spatially constrained permutation tests[96,97]. We performed 1000 permutations of the labels of patients vs. controls, computed a corresponding null ICC matrix for the patients and controls groups, and estimated the correlation of the resulting random differences in ICC for these null models with each of the 19 neurotransmitter atlas maps.

Data availability

The data are available through the Clinical Biospecimen Imaging and Genetic (C-BIG) repository (https://www.mcgill.ca/neuro/open-science/c-big-repository)[85], the PREVENT-AD open resource (https://openpreventad.loris.ca/ and https://registeredpreventad.loris.ca)[86], and the OMEGA repository (https://www.mcgill.ca/bic/resources/omega)[22]. Normative neurotransmitter density data are available from *neuromaps* (https://github.com/netneurolab/neuromaps)[36].

Code availability

All in-house code used for data analysis and visualization is available on GitHub https://github.com/jasondsc/PDneuralfingerprinting.

Acknowledgements

Data collection and sharing for this project was provided by the Quebec Parkinson Network (QPN), the Pre-symptomatic Evaluation of Novel or Experimental Treatments for Alzheimer's Disease (PREVENT-AD; release 6.0) program, and the Open MEG Archives (OMEGA). The funders had no role in study design, data collection and analysis, decision to publish, or preparation of the manuscript. The QPN is funded by a grant from Fonds de recherche du Québec - Santé (FRQS). PREVENT-AD was launched in 2011 as a $13.5 million, 7-year public-private partnership using funds provided by McGill University, the FRQS, an unrestricted research grant from Pfizer Canada, the Levesque Foundation, the Douglas Hospital Research Centre and Foundation, the Government of Canada, and the Canada Fund for Innovation. Private sector contributions

are facilitated by the Development Office of the McGill University Faculty of Medicine and by the Douglas Hospital Research Centre Foundation (http://www.douglas.qc.ca/). OMEGA and the Brainstorm app are supported by funding to SB from the NIH (R01-EB026299), a Discovery grant from the Natural Science and Engineering Research Council of Canada (436355-13), the CIHR Canada research Chair in Neural Dynamics of Brain Systems, the Brain Canada Foundation with support from Health Canada, and the Innovative Ideas program from the Canada First Research Excellence Fund, awarded to McGill University for the HBHL initiative. This work was supported by a grant F32-NS119375 (AIW) from the National Institutes of Health and a doctoral fellowship from NSERC (JDSC, JYH).

References

1. Stoffers, D. *et al.* Slowing of oscillatory brain activity is a stable characteristic of Parkinson's disease without dementia. *Brain* **130**, 1847–1860 (2007).

2. Stoffers, D., Bosboom, J. L. W., Wolters, E. Ch., Stam, C. J. & Berendse, H. W. Dopaminergic modulation of cortico-cortical functional connectivity in Parkinson's disease: An MEG study. *Exp. Neurol.* **213**, 191–195 (2008).

3. Bosboom, J. L. W. *et al.* Resting state oscillatory brain dynamics in Parkinson's disease: An MEG study. *Clin. Neurophysiol.* **117**, 2521–2531 (2006).

4. Jubault, T. *et al.* Patterns of cortical thickness and surface area in early Parkinson's disease. *NeuroImage* **55**, 462–467 (2011).

5. Hanganu, A. *et al.* Mild cognitive impairment is linked with faster rate of cortical thinning in patients with Parkinson's disease longitudinally. *Brain J. Neurol.* **137**, 1120–1129 (2014).

6. Wilson, H., Niccolini, F., Pellicano, C. & Politis, M. Cortical thinning across Parkinson's disease stages and clinical correlates. *J. Neurol. Sci.* **398**, 31–38 (2019).

7. Pereira, J. B. *et al.* Initial cognitive decline is associated with cortical thinning in early Parkinson disease. *Neurology* **82**, 2017–2025 (2014).

8. Tinkhauser, G. *et al.* Beta burst dynamics in Parkinson's disease OFF and ON dopaminergic medication. *Brain J. Neurol.* **140**, 2968–2981 (2017).

9. Torrecillos, F. *et al.* Modulation of Beta Bursts in the Subthalamic Nucleus Predicts Motor Performance. *J. Neurosci. Off. J. Soc. Neurosci.* **38**, 8905–8917 (2018).

10. Yu, Y. *et al.* Parkinsonism Alters Beta Burst Dynamics across the Basal Ganglia-Motor Cortical Network. *J. Neurosci. Off. J. Soc. Neurosci.* **41**, 2274–2286 (2021).

11. Olde Dubbelink, K. T. E. *et al.* Cognitive decline in Parkinson's disease is associated with slowing of resting-state brain activity: a longitudinal study. *Neurobiol. Aging* **34**, 408–418 (2013).

12. Wiesman, A. I. *et al.* A sagittal gradient of pathological and compensatory effects of neurophysiological slowing in Parkinson's disease. 2022.08.05.22278436 Preprint at https://doi.org/10.1101/2022.08.05.22278436 (2022).

13. Kim, J. *et al.* Abnormal intrinsic brain functional network dynamics in Parkinson's disease. *Brain* **140**, 2955–2967 (2017).

14. Zhu, H. *et al.* Abnormal Dynamic Functional Connectivity Associated With Subcortical Networks in Parkinson's Disease: A Temporal Variability Perspective. *Front. Neurosci.* **13**, (2019).

15. Fiorenzato, E. *et al.* Dynamic functional connectivity changes associated with dementia in Parkinson's disease. *Brain* **142**, 2860–2872 (2019).

16. Díez-Cirarda, M. *et al.* Dynamic functional connectivity in Parkinson's disease patients with mild cognitive impairment and normal cognition. *NeuroImage Clin.* **17**, 847–855 (2018).

17. Finn, E. S. *et al.* Functional connectome fingerprinting: identifying individuals using patterns of brain connectivity. *Nat. Neurosci.* **18**, 1664–1671 (2015).

18. Amico, E. & Goñi, J. The quest for identifiability in human functional connectomes. *Sci. Rep.* **8**, 8254 (2018).

19. Rosenberg, M. D., Finn, E. S., Scheinost, D., Constable, R. T. & Chun, M. M. Characterizing Attention with Predictive Network Models. *Trends Cogn. Sci.* **21**, 290–302 (2017).

20. Greene, A. S., Gao, S., Scheinost, D. & Constable, R. T. Task-induced brain state manipulation improves prediction of individual traits. *Nat. Commun.* **9**, 2807 (2018).

21. da Silva Castanheira, J., Orozco Perez, H. D., Misic, B. & Baillet, S. Brief segments of neurophysiological activity enable individual differentiation. *Nat. Commun.* **12**, 5713 (2021).

22. Niso, G. *et al.* OMEGA: The Open MEG Archive. *NeuroImage* **124**, 1182–1187 (2016).

23. Poldrack, R. A. & Gorgolewski, K. J. Making big data open: data sharing in neuroimaging. *Nat. Neurosci.* **17**, 1510–1517 (2014).

24. Sareen, E. *et al.* Exploring MEG brain fingerprints: Evaluation, pitfalls, and interpretations. *NeuroImage* **240**, 118331 (2021).

25. Sorrentino, P. *et al.* Clinical connectome fingerprints of cognitive decline. *NeuroImage* **238**, 118253 (2021).

27. Kaufmann, T. *et al.* Delayed stabilization and individualization in connectome development are related to psychiatric disorders. *Nat. Neurosci.* **20**, 513–515 (2017).

28. Kaufmann, T. *et al.* Stability of the Brain Functional Connectome Fingerprint in Individuals With Schizophrenia. *JAMA Psychiatry* **75**, 749 (2018).

29. Maidan, I. *et al.* Neural Variability in the Prefrontal Cortex as a Reflection of Neural Flexibility and Stability in Patients With Parkinson Disease. *Neurology* **98**, e839–e847 (2022).

30. Shafiei, G., Baillet, S. & Misic, B. Human electromagnetic and haemodynamic networks systematically converge in unimodal cortex and diverge in transmodal cortex. *PLoS Biol.* **20**, e3001735 (2022).

31. Troisi Lopez, E. *et al.* Fading of brain network fingerprint in Parkinson's disease predicts motor clinical impairment. *Hum. Brain Mapp.* **n/a**,.

32. Sadaghiani, S., Brookes, M. J. & Baillet, S. Connectomics of human electrophysiology. *NeuroImage* **247**, 118788 (2022).

33. Donoghue, T. *et al.* Parameterizing neural power spectra into periodic and aperiodic components. *Nat. Neurosci.* **23**, 1655–1665 (2020).

34. Wilson, L. E., da Silva Castanheira, J. & Baillet, S. Time-resolved parameterization of aperiodic and periodic brain activity. *eLife* **11**, e77348 (2022).

35. Margulies, D. S. *et al.* Situating the default-mode network along a principal gradient of macroscale cortical organization. *Proc. Natl. Acad. Sci.* **113**, 12574–12579 (2016).

36. Markello, R. D. *et al.* neuromaps: structural and functional interpretation of brain maps. *Nat. Methods* **19**, 1472–1479 (2022).

37. Baillet, S. Magnetoencephalography for brain electrophysiology and imaging. *Nat. Neurosci.* **20**, 327–339 (2017).

38. Desikan, R. S. *et al.* An automated labeling system for subdividing the human cerebral cortex on MRI scans into gyral based regions of interest. *NeuroImage* **31**, 968–980 (2006).

39. da Silva Castanheira, J., Orozco Perez, H. D., Misic, B. & Baillet, S. Brief segments of neurophysiological activity enable individual differentiation. *Nat. Commun.* **12**, 5713 (2021).

40. Shrout, P. E. & Fleiss, J. L. Intraclass correlations: Uses in assessing rater reliability. *Psychol. Bull.* **86**, 420–428 (1979).

41. John, C. R. *et al. M3C: Monte Carlo reference-based consensus clustering*. http://biorxiv.org/lookup/doi/10.1101/377002 (2018) doi:10.1101/377002.

42. *Model Selection and Multimodel Inference*. (Springer, 2004). doi:10.1007/b97636.

43. Hoehn, M. M. & Yahr, M. D. Parkinsonism: onset, progression, and mortality. *Neurology* **17**, 427–427 (1967).

44. Goetz, C. G. *et al. Movement* Disorder Society Task Force report on the Hoehn and Yahr staging scale: Status and recommendations The *Movement* Disorder Society Task Force on rating scales for Parkinson's disease. *Mov. Disord.* **19**, 1020–1028 (2004).

45. Rosenberg, M. D. *et al.* Functional connectivity predicts changes in attention observed across minutes, days, and months. *Proc. Natl. Acad. Sci. U. S. A.* **117**, 3797–3807 (2020).

46. Burton, C. L., Strauss, E., Hultsch, D. F., Moll, A. & Hunter, M. A. Intraindividual Variability as a Marker of Neurological Dysfunction: A Comparison of Alzheimer's Disease and Parkinson's Disease. *J. Clin. Exp. Neuropsychol.* **28**, 67–83 (2006).

47. Costa, A. S., Dogan, I., Schulz, J. B. & Reetz, K. Going beyond the mean: Intraindividual variability of cognitive performance in prodromal and early neurodegenerative disorders. *Clin. Neuropsychol.* **33**, 369–389 (2019).

48. Singh, A. *et al.* Timing variability and midfrontal ~4 Hz rhythms correlate with cognition in Parkinson's disease. *Npj Park. Dis.* **7**, 14 (2021).

49. Jones, J. D., Valenzuela, Y. G., Uribe, C., Bunch, J. & Kuhn, T. P. Intraindividual variability in neuropsychological performance predicts longitudinal cortical volume loss in early Parkinson's disease. *Neuropsychology* **36**, 513–519 (2022).

50. Nomi, J. S., Bolt, T. S., Ezie, C. E. C., Uddin, L. Q. & Heller, A. S. Moment-to-Moment BOLD Signal Variability Reflects Regional Changes in Neural Flexibility across the Lifespan. *J. Neurosci.* **37**, 5539–5548 (2017).

51. Garrett, D. D., Kovacevic, N., McIntosh, A. R. & Grady, C. L. Blood Oxygen Level-Dependent Signal Variability Is More than Just Noise. *J. Neurosci.* **30**, 4914–4921 (2010).

52. Garrett, D. D., Kovacevic, N., McIntosh, A. R. & Grady, C. L. The modulation of BOLD variability between cognitive states varies by age and processing speed. *Cereb. Cortex N. Y. N 1991* **23**, 684–693 (2013).

53. Li, S. C., Lindenberger, U. & Sikström, S. Aging cognition: from neuromodulation to representation. *Trends Cogn. Sci.* **5**, 479–486 (2001).

54. MacDonald, S. W. S., Li, S.-C. & Bäckman, L. Neural underpinnings of within-person variability in cognitive functioning. *Psychol. Aging* **24**, 792–808 (2009).

55. Geraedts, V. J. *et al.* Clinical correlates of quantitative EEG in Parkinson disease: A systematic review. *Neurology* **91**, 871–883 (2018).

56. Oswal, A., Brown, P. & Litvak, V. Synchronized neural oscillations and the pathophysiology of Parkinson's disease: *Curr. Opin. Neurol.* **26**, 662–670 (2013).

57. Wilkinson, J. L. Cerebral cortex. in *Neuroanatomy for Medical Students* 215–234 (Elsevier, 1992). doi:10.1016/B978-0-7506-1447-4.50016-5.

58. Caspers, S. & Zilles, K. Microarchitecture and connectivity of the parietal lobe. in *Handbook of Clinical Neurology* vol. 151 53–72 (Elsevier, 2018).

59. Rusconi, E. Gerstmann syndrome: historic and current perspectives. in *Handbook of Clinical Neurology* vol. 151 395–411 (Elsevier, 2018).

60. Unnithan, A. K. A. & Emmady, P. D. Astereognosis. in *StatPearls* (StatPearls Publishing, 2022).

61. Menon, V. & Desmond, J. E. Left superior parietal cortex involvement in writing: integrating fMRI with lesion evidence. *Cogn. Brain Res.* **12**, 337–340 (2001).

62. Koenigs, M., Barbey, A. K., Postle, B. R. & Grafman, J. Superior Parietal Cortex Is Critical for the Manipulation of Information in Working Memory. *J. Neurosci.* **29**, 14980–14986 (2009).

63. Culham, J. C., Cavina-Pratesi, C. & Singhal, A. The role of parietal cortex in visuomotor control: what have we learned from neuroimaging? *Neuropsychologia* **44**, 2668–2684 (2006).

64. Passarelli, L., Gamberini, M. & Fattori, P. The superior parietal lobule of primates: a sensory-motor hub for interaction with the environment. *J. Integr. Neurosci.* **20**, 157–171 (2021).

65. Wager, T. D. & Smith, E. E. Neuroimaging studies of working memory: *Cogn. Affect. Behav. Neurosci.* **3**, 255–274 (2003).

66. Koenigs, M., Barbey, A. K., Postle, B. R. & Grafman, J. Superior Parietal Cortex Is Critical for the Manipulation of Information in Working Memory. *J. Neurosci.* **29**, 14980–14986 (2009).

67. Kim, J. *et al.* Dopamine depletion can be predicted by the aperiodic component of subthalamic local field potentials. *Neurobiol. Dis.* **168**, 105692 (2022).

68. Belova, E. M., Semenova, U., Gamaleya, A. A., Tomskiy, A. A. & Sedov, A. Voluntary movements cause beta oscillations increase and broadband slope decrease in the subthalamic nucleus of parkinsonian patients. *Eur. J. Neurosci.* **53**, 2205–2213 (2021).

69. Guerra, A. *et al.* Enhancing Gamma Oscillations Restores Primary Motor Cortex Plasticity in Parkinson's Disease. *J. Neurosci.* **40**, 4788–4796 (2020).

70. Underwood, C. F. & Parr-Brownlie, L. C. Primary motor cortex in Parkinson's disease: Functional changes and opportunities for neurostimulation. *Neurobiol. Dis.* **147**, 105159 (2021).

71. Tessitore, A. *et al.* Default-mode network connectivity in cognitively unimpaired patients with Parkinson disease. *Neurology* **79**, 2226–2232 (2012).

72. van Eimeren, T., Monchi, O., Ballanger, B. & Strafella, A. P. Dysfunction of the Default Mode Network in Parkinson Disease: A Functional Magnetic Resonance Imaging Study. *Arch. Neurol.* **66**, 877–883 (2009).

73. Ruppert, M. C. *et al.* The default mode network and cognition in Parkinson's disease: A multimodal resting-state network approach. *Hum. Brain Mapp.* **42**, 2623–2641 (2021).

74. Lucas-Jiménez, O. *et al.* Altered functional connectivity in the default mode network is associated with cognitive impairment and brain anatomical changes in Parkinson's disease. *Parkinsonism Relat. Disord.* **33**, 58–64 (2016).

75. Krajcovicova, L., Mikl, M., Marecek, R. & Rektorova, I. The default mode network integrity in patients with Parkinson's disease is levodopa equivalent dose-dependent. *J. Neural Transm.* **119**, 443–454 (2012).

76. Delaveau, P. *et al.* Dopaminergic modulation of the default mode network in Parkinson's disease. *Eur. Neuropsychopharmacol.* **20**, 784–792 (2010).

77. Narayanan, N. S., Rodnitzky, R. L. & Uc, E. Y. Prefrontal dopamine signaling and cognitive symptoms of Parkinson's disease. *Rev. Neurosci.* **24**, (2013).

78. Poewe, W. *et al.* Parkinson disease. *Nat. Rev. Dis. Primer* **3**, 1–21 (2017).

79. Gerdeman, G. L., Ronesi, J. & Lovinger, D. M. Postsynaptic endocannabinoid release is critical to long-term depression in the striatum. *Nat. Neurosci.* **5**, 446–451 (2002).

80. Hohmann, A. G. & Herkenham, M. Localization of cannabinoid CB1 receptor mRNA in neuronal subpopulations of rat striatum: A double-label in situ hybridization study. *Synapse* **37**, 71–80 (2000).

81. Brotchie, J. CB cannabinoid receptor signalling in Parkinson's disease. *Curr. Opin. Pharmacol.* **3**, 54–61 (2003).

82. Kuntsi, J. & Klein, C. Intraindividual Variability in ADHD and Its Implications for Research of Causal Links. in *Behavioral Neuroscience of Attention Deficit Hyperactivity Disorder and Its Treatment* (eds. Stanford, C. & Tannock, R.) vol. 9 67–91 (Springer Berlin Heidelberg, 2011).

83. Wiesman, A. I., da Silva Castanheira, J. & Baillet, S. Stability of spectral estimates in resting-state magnetoencephalography: Recommendations for minimal data duration with neuroanatomical specificity. *NeuroImage* **247**, 118823 (2022).

84. Van Horn, J. D., Grafton, S. T. & Miller, M. B. Individual Variability in Brain Activity: A Nuisance or an Opportunity? *Brain Imaging Behav.* **2**, 327 (2008).

85. Gan-Or, Z. *et al.* The Quebec Parkinson Network: A Researcher-Patient Matching Platform and Multimodal Biorepository. *J. Park. Dis.* **10**, 301–313 (2020).

86. Tremblay-Mercier, J. *et al.* Open science datasets from PREVENT-AD, a longitudinal cohort of pre-symptomatic Alzheimer's disease. *NeuroImage Clin.* **31**, 102733 (2021).

87. Tadel, F., Baillet, S., Mosher, J. C., Pantazis, D. & Leahy, R. M. Brainstorm: A User-Friendly Application for MEG/EEG Analysis. *Comput. Intell. Neurosci.* **2011**, 1–13 (2011).

88. Gross, J. *et al.* Good practice for conducting and reporting MEG research. *NeuroImage* **65**, 349–363 (2013).

89. Wiesman, A. I. *et al. Aberrant neurophysiological signaling underlies speech impairments in Parkinson's disease*. http://medrxiv.org/lookup/doi/10.1101/2022.04.01.22273315 (2022) doi:10.1101/2022.04.01.22273315.

90. Fischl, B. FreeSurfer. *NeuroImage* **62**, 774–781 (2012).

91. Goetz, C. G. *et al.* Movement Disorder Society-sponsored revision of the Unified Parkinson's Disease Rating Scale (MDS-UPDRS): Scale presentation and clinimetric testing results: MDS-UPDRS: Clinimetric Assessment. *Mov. Disord.* **23**, 2129–2170 (2008).

92. Nasreddine, Z. S. *et al.* The Montreal Cognitive Assessment, MoCA: A Brief Screening Tool For Mild Cognitive Impairment: MOCA: A BRIEF SCREENING TOOL FOR MCI. *J. Am. Geriatr. Soc.* **53**, 695–699 (2005).

93. Cook, R. D. Detection of Influential Observation in Linear Regression. *Technometrics* **19**, 15–18 (1977).

94. Lüdecke, D., Ben-Shachar, M., Patil, I., Waggoner, P. & Makowski, D. performance: An R Package for Assessment, Comparison and Testing of Statistical Models. *J. Open Source Softw.* **6**, 3139 (2021).

95. Yeo, Thomas, B. T. *et al.* The organization of the human cerebral cortex estimated by intrinsic functional connectivity. *J. Neurophysiol.* **106**, 1125–1165 (2011).

96. Markello, R. D. & Misic, B. Comparing spatial null models for brain maps. *NeuroImage* **236**, 118052 (2021).

97. Váša, F. & Mišić, B. Null models in network neuroscience. *Nat. Rev. Neurosci.* **23**, 493–504 (2022).

98. R Core Team. *R: A Language and Environment for Statistical Computing*. (R Foundation for Statistical Computing, 2022).

Supplemental Information

Participants.

The study participants are patients with Parkinson's disease and age-matched healthy controls from the OMEGA, PREVENT-AD, and QPN data repositories[1–3]. Table S1 provides their demographics, which we tested for sample differences in terms of age and education, using an unpaired t-test and gender and handedness with a Chi-square test. No significant differences were found.

	Patients	*Controls*	*Uncorrected p-values*
age	64.63 (8.66)	61.98 (8.89)	0.09
gender (female)	23	24	0.13
handedness (right)	67	48	1.0
education	15.11 (3.11)	15.54 (3.58)	0.48
Hoehn & Yahr score	1.97 (0.71)	NA	
UPDRS III	32.55 (14.74)	NA	
MoCA	24.43 (4.03)	NA	

Table S1: Participant demographics.

Individual differentiation from distinct spectral features of the brain-fingerprint.

These individual differentiations accuracies between controls, patients and patients vs. Controls are reported in Figure S1, based on the original broadband spectral brain-fingerprints ("broadband"), their arhythmic components ("arhythmic") and the arhythmic-corrected versions ("arhythmic corrected").

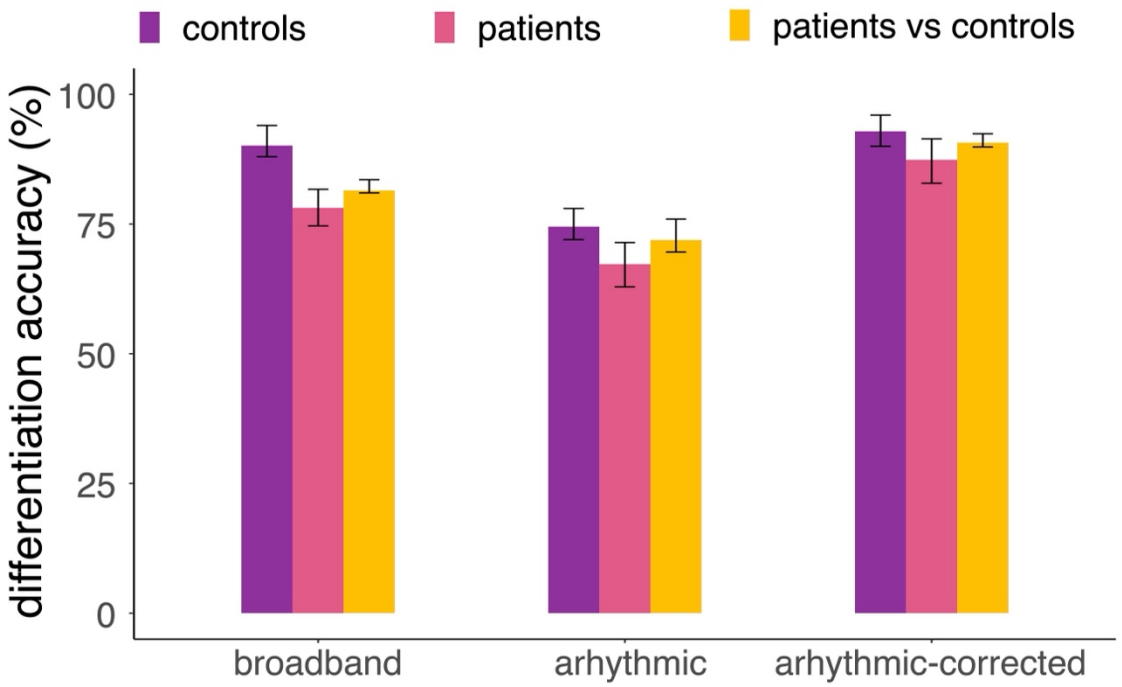

Figure S1: Individual differentiation from distinct spectral features of the brain-fingerprint. Error bars are from bootstrapped estimates of individual differentiation accuracies (see Methods).

Figure S2 depicts the t-SNE 2-D projection of each participant' brain-fingerprints (two per participant). The dashed lines connect the two brain-fingerprints of each participant (see Figure 2c for a subset of participants), which may not be visible in participants with highly consistent brain-fingerprints derived from two distinct datasets.

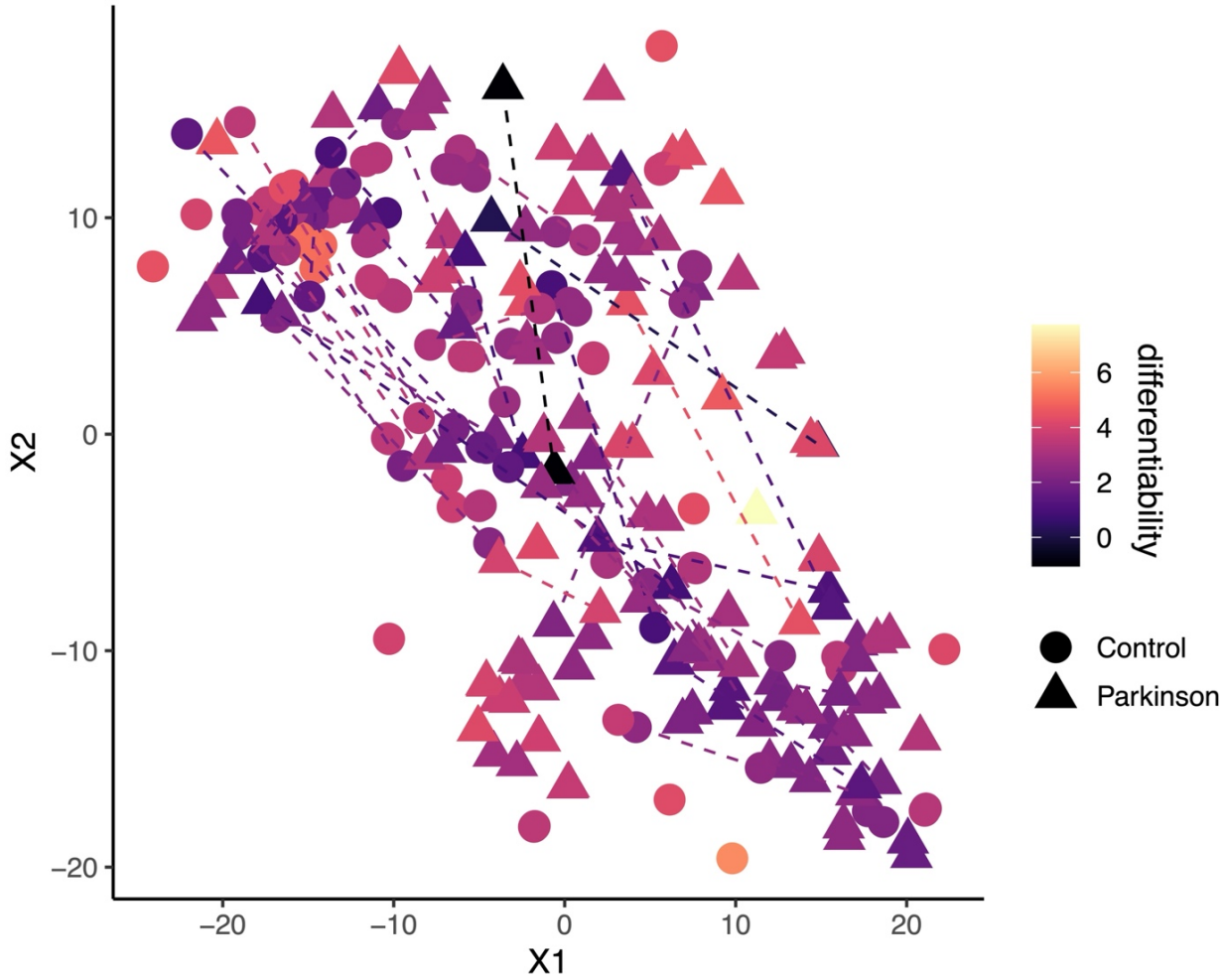

Figure S2: t-SNE map of all participants (N=133)

t-SNE mapping of individual spectral brain-fingerprints for display of all participants. Dotted lines connect between the two spectral brain-fingerprints derived from the two non-overlapping datasets used to produce the spectral brain-fingerprints of each participant. Note that dotted lines are not visible in participants with stable brain-fingerprints (plots overlap). We found that the 2-D Euclidian distances between each participant's two spectral brain-fingerprints in this 2-D space scaled linearly with the differentiability. The smaller the distance between low-dimensional representations of the individual's spectral brain-fingerprints, the more differentiable are the participants (see Figure 2c).

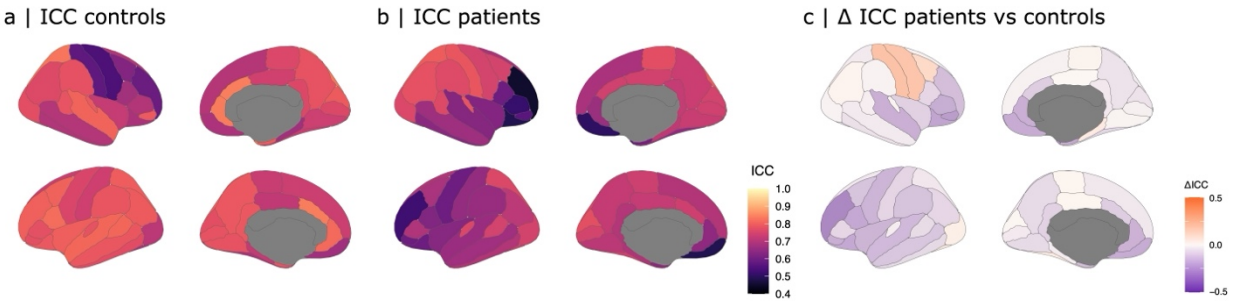

Figure S3: Relative contribution of features for fingerprinting

Intra-class correlation coefficients (ICCs) plotted for (a) the within control cohort fingerprinting challenge, (b) the PD patient cohort challenge, and (c) the difference between the PD and control challenge.

Environmental artifacts and possible neuroanatomical confounds.

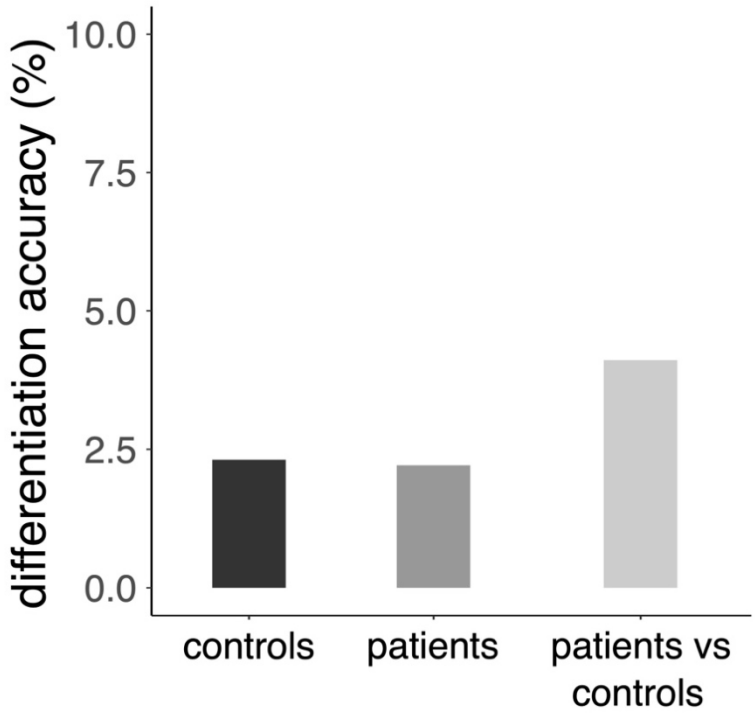

Figure S4: Differentiation accuracy from empty-room data.

Differentiation accuracies from brain-fingerprints derived from empty-room recordings performed around the MEG visit of each participant.

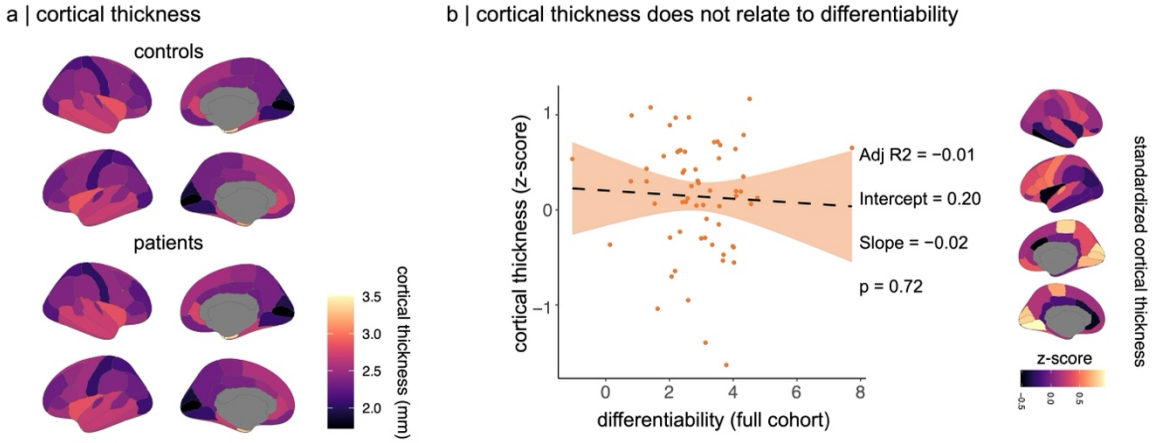

Figure S5: (a) Average cortical thickness measured in control participants and patients with PD. (b) left panel: linear regression analysis showing no relationship between individual differentiability and the average standardized cortical thickness of each patient (averaged across ROIs) (see Methods). Right panel: brain maps of average standardized cortical thickness of patients with PD.

Differentiability of patients with PD is correlated to head motion (r= 0.23, *p*= 0.04), but not to cardiac or ocular artifacts (r= -0.04, *p*= 0.71; r= -0.08, *p*= 0.46 respectively). There was, however, little evidence in favour of the relationship between head motion and differentiability (BF= 2.04; Figure S6).

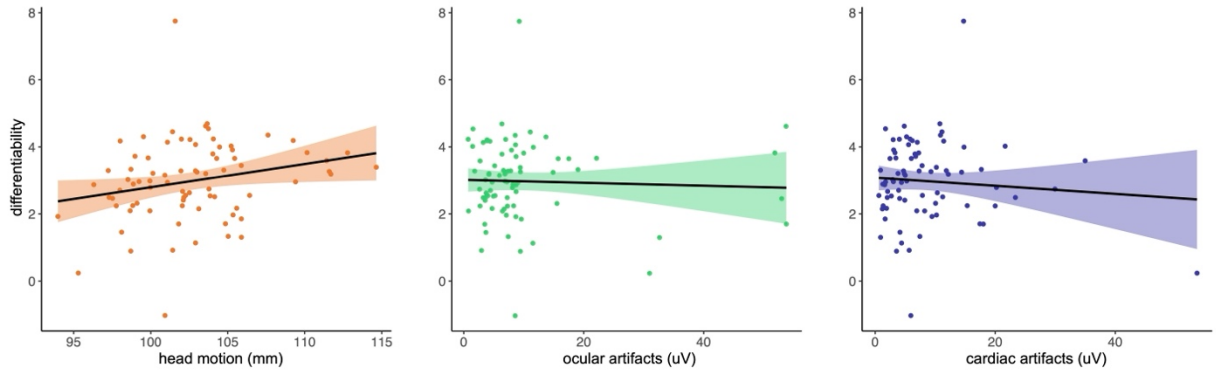

Figure S6: Individual differentiability does not relate to cardiac or ocular artifacts (middle and right panels). A moderate linear relationship exists between individual differentiability and head motion in the patient group.

Individual differentiation relates to motor and cognitive symptoms

We hypothesized that patient differentiation scales with the severity of motor symptoms. We fit linear regression models to predict individual differentiability from UPDRS III[8] scores (Tables S2 & S3). Table S4 details the interaction between motor and cognitive symptoms in predicting differentiability.

Table S2: Differentiability and motor symptoms, with head motion as covariate.

	differentiability			
predictors	*estimates*	*CI*	*p*	*BF*
intercept	2.14	-0.93 – 5.02	0.174	
age	-0.01	-0.05 – 0.03	0.503	2.02
education coded	0.06	-0.04 – 0.16	0.236	1.35
disease duration	-0.04	-0.12 – 0.03	0.231	1.33
UPDRS	0.03	0.01 – 0.06	0.004	0.07
observations	56			
R^2 / R^2 adjusted	0.187 / 0.123			

Table S3: Differentiability and motor-cognitive interaction.

	differentiability			
predictors	*estimates*	*CI*	*p*	*BF*
intercept	-6.02	-12.50 – 6.44	0.523	
age	-0.00	-0.05 – 0.05	0.998	2.16
education coded	0.05	-0.05 – 0.15	0.307	1.41
disease duration	-0.04	-0.11 – 0.03	0.301	1.39
head motion	0.05	-0.03 – 0.14	0.207	1.13
UPDRS	0.00	-0.03 – 0.04	0.903	2.16
MoCA	-2.25	-3.96 – -0.55	0.011	0.16
UPDRS * MoCA	0.06	0.01 – 0.10	0.025	0.28
observations	56			

R^2 / R^2 adjusted	0.294 / 0.191

Differentiation of patients from arhythmic brain activity relates to motor symptoms

Individual differentiability from the arhythmic components of the brain-fingerprint is also associated with motor symptoms (Figure S7and Table S5). The left superior parietal cortex remains the most salient cortical region in this relationship (Figure S8). There was no interaction between the motor and cognitive symptoms in predicting individual differentiability from the arhythmic components of the brain-fingerprint (Table S6).

Individual differentiability from arhythmic-corrected brain-fingerprints is not related to the severity of motor symptoms (Tables S7 & S8).

Table S4: Individual differentiability from arhythmic spectral brain-fingerprints and association with motor symptoms.

	differentiability			
predictors	*estimates*	*CI*	*p*	*BF*
intercept	1.91	-4.61 – 8.44	0.558	
age	-0.03	-0.06 – 0.00	0.055	0.47
education coded	0.03	-0.04 – 0.10	0.407	1.52
disease duration	-0.01	-0.06 – 0.04	0.811	1.95
head motion	-0.00	-0.06 – 0.05	0.931	1.99
UPDRS	0.02	0.00 – 0.04	**0.033**	0.34
specparam fit	1.62	-0.75 – 3.99	0.176	0.97
observations	56			
R^2 / R^2 adjusted	0.163 / 0.061			

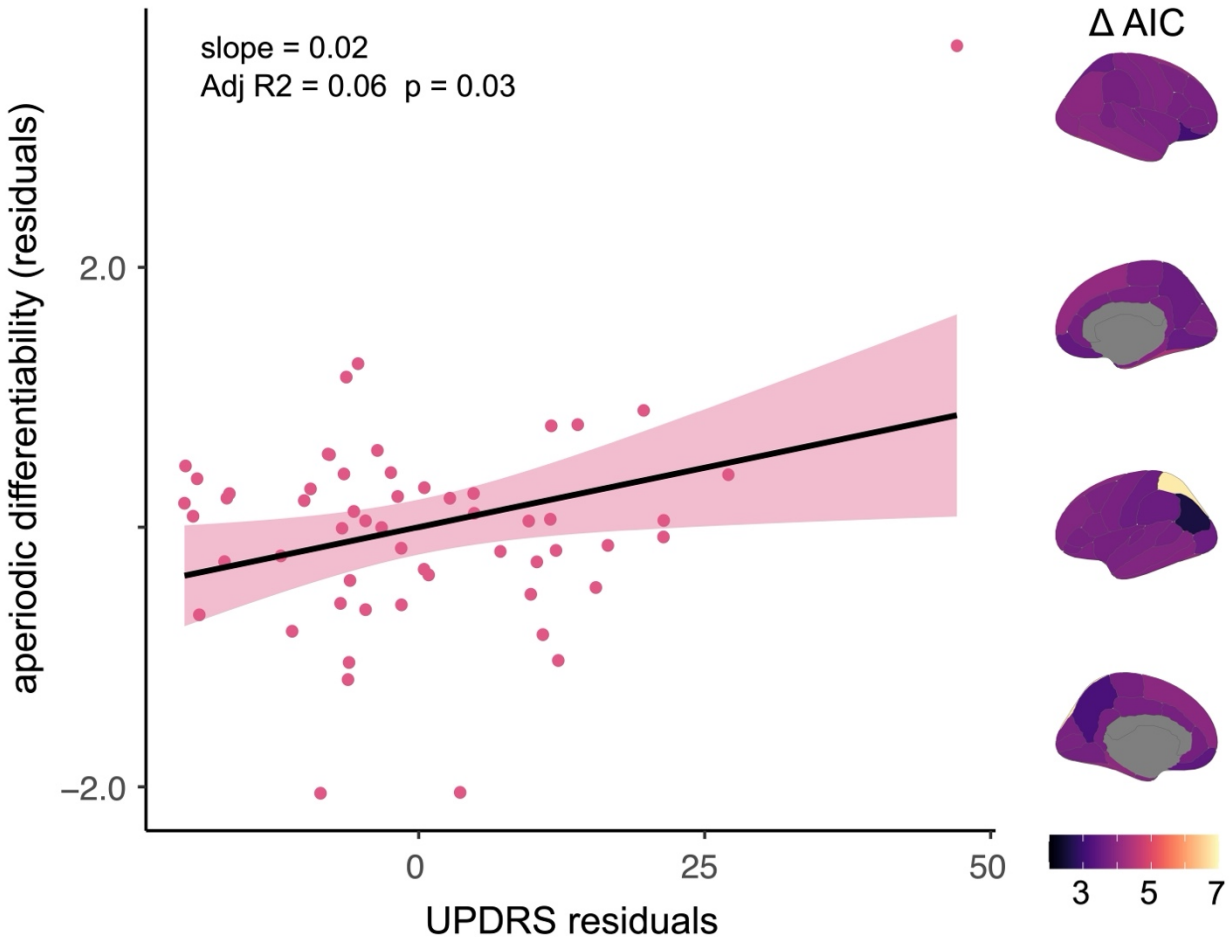

Figure S7: Individual differentiability from arhythmic and arhythmic-corrected spectral brain-fingerprints and relations to motor symptoms.

Left panel: the differentiability of patients from arhythmic spectral brain-fingerprints is associated with the severity of their motor symptoms measured on the UPDRS part III scale. Right panel: The relative changes of Akaike's information criterion (ΔAIC) depict which region(s) of the arhythmic brain-fingerprint contributes the most to the association between individual differentiability and PD motor symptoms. We found that only the left superior parietal cortex contributes to the association between individual arrhythmic differentiability and the severity of motor symptoms.

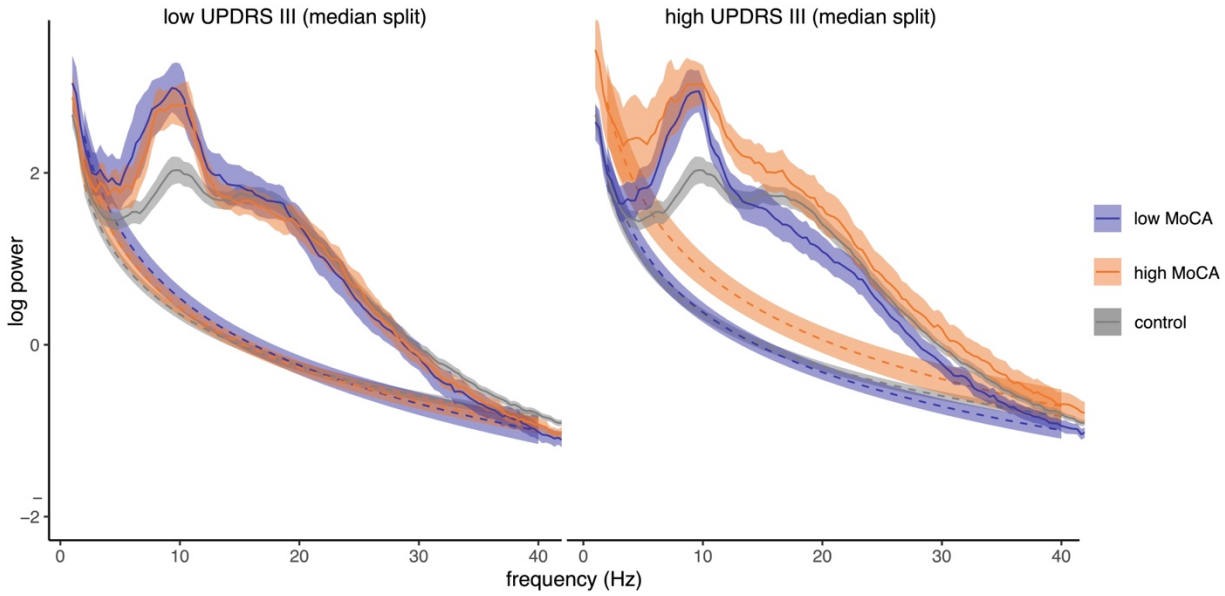

Figure S8: Parameterized spectra from left superior parietal cortex.

Spectral power (solid lines) and arhythmic spectral power (dashed lines) in the left superior parietal cortex of participants with high and low MoCA[9] scores and high and low UPDRS[8] scores, respectively. Patients presenting high vs. low MoCA scores are shown with different colors, and with high vs. low UPDRS III scores (left vs. right graphs) using median splits of the cohort, for visualization. Shaded regions depict the standard error on the mean.

Table S5: Motor-cognitive interaction in the association of individual differentiability from arhythmic spectral brain-fingerprints and motor symptoms.

	differentiability			
predictors	*estimates*	*CI*	*p*	*BF*
intercept	0.66	-6.21 – 7.54	0.847	
age	-0.03	-0.06 – 0.01	0.139	0.80
education coded	0.03	-0.04 – 0.10	0.425	1.44
disease duration	-0.00	-0.05 – 0.05	0.898	1.83
head motion	0.01	-0.05 – 0.07	0.703	1.74
specparam fit	1.60	-0.91 – 4.11	0.206	0.99
UPDRS	0.01	-0.02 – 0.03	0.526	1.84
MoCA	-0.77	-2.00 – 0.46	0.213	1.02
UPDRS * MoCA	0.02	-0.02 – 0.05	0.287	1.19
observations	56			
R^2 / R^2 adjusted	0.191 / 0.054			

Table S6: Individual differentiability from arhythmic-corrected spectral brain-fingerprints not associated with motor symptoms.

	differentiability			
predictors	*estimates*	*CI*	*p*	*BF*
intercept	5.19	-6.50 – 16.88	0.377	
age	-0.03	-0.09 – 0.03	0.298	1.24
education coded	0.05	-0.08 – 0.18	0.456	1.51
disease duration	0.02	-0.07 – 0.11	0.594	1.68
head motion	-0.03	-0.13 – 0.07	0.534	1.61
UPDRS	0.03	-0.00 – 0.06	0.062	0.50
specparam fit	2.55	-1.70 – 6.80	0.234	1.09
observations	56			
R^2 / R^2 adjusted	0.097 /- 0.014			

Table S7: Motor-cognitive interaction in the association of individual differentiability from arhythmic-corrected spectral brain-fingerprints and motor symptoms.

		differentiability		
predictors	*estimates*	*CI*	*p*	*BF*
intercept	1.38	-10.56 – 13.31	0.817	
age	-0.02	-0.08 – 0.05	0.617	1.66
education coded	0.05	-0.08 – 0.18	0.451	1.47
disease duration	0.03	-0.06 – 0.12	0.472	1.50
head motion	0.01	-0.10 – 0.12	0.850	1.80
specparam fit	2.35	-2.00 – 6.71	0.282	1.18
UPDRS	-0.00	-0.05 – 0.04	0.861	1.82
MoCA	-2.31	-4.45 – -0.18	0.034	0.34
UPDRS * MoCA	0.06	-0.00 – 0.12	0.058	0.47
observations	56			
R^2 / R^2 adjusted	0.166 / 0.024			

Decoding of disease staging relates to salient features of the spectral brain-fingerprint.

The ability to decode disease stages from regional brain-fingerprint features is correlated with the related changes in ICC between patients and controls differentiation (see Figure 5a-c).

To verify that this result was not biased by the 80-20 cross-validation strategy, we replicated the approach using 90-10 and 70-30 cross-validations (e.g., using 90% of the data to train the decoder and 10% to test its performance) and found qualitatively similar results (Figure S9).

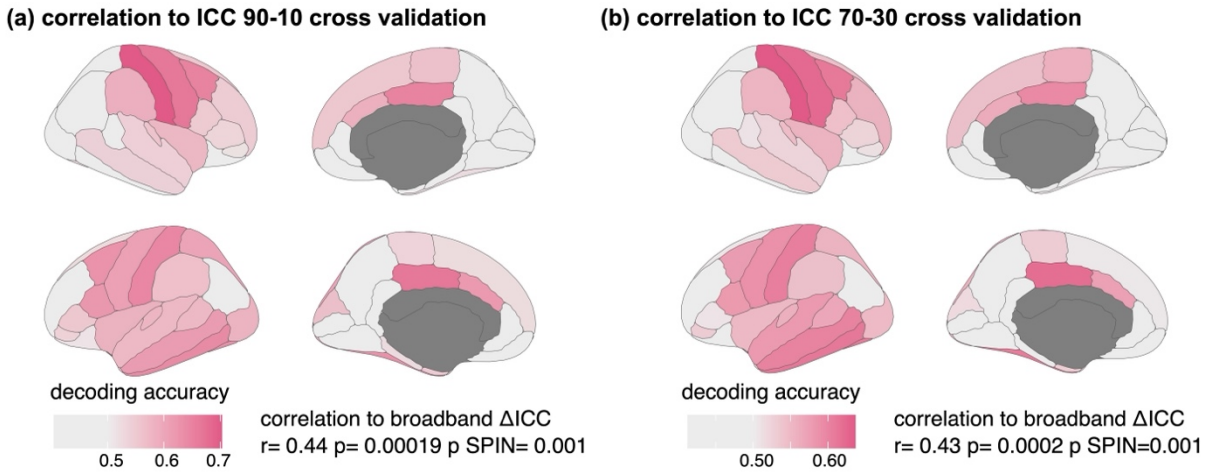

Figure S9: Decoding of disease stages does not depend on cross-validation strategy.
Topography of decoding accuracies of Parkinson's disease stages (binarized Hoehn & Yahr scores) from the spectral brain-fingerprint features of each cortical parcel. The observed topography remains similar regardless of the cross-validation method. The decoding accuracy of Parkinson's disease stages at each cortical parcel remains correlated to the saliency of the brain-fingerprints of each cortical parcel (Δ ICC, right; Figure 4b right panel) regardless of the cross-validation method.

Table S8: Differentiation accuracy derived from shorter (30-s) datasets exhibits pronounced short-term variability of patient brain-fingerprints.

	differentiation accuracy			
predictors	*estimates*	*CI*	*p*	*BF*
intercept	94.57	92.01 – 96.79	<0.001	
gap duration between brain-fingerprints	-2.07	-2.53 – -1.62	<0.001	4.22e-56
group [*within PD*]	-0.73	-4.30 – 2.83	0.686	9.28e-11
group [*PD Vs HC*]	2.32	-1.24 – 5.89	0.201	9.28e-11
gap duration between brain-fingerprints * group [*within PD*]	-1.48	-2.13 – -0.84	<0.001	2.86e-3
gap duration between brain-fingerprints * group [*PD vs HC*]	-1.29	-1.94 – -0.65	<0.001	2.86e-3
observations	234			
R^2 / R^2 adjusted	0.721 / 0.715			

References

1. Niso, G. *et al.* OMEGA: The Open MEG Archive. *NeuroImage* **124**, 1182–1187 (2016).
2. Tremblay-Mercier, J. *et al.* Open science datasets from PREVENT-AD, a longitudinal cohort of pre-symptomatic Alzheimer's disease. *NeuroImage Clin.* **31**, 102733 (2021).
3. Gan-Or, Z. *et al.* The Quebec Parkinson Network: A Researcher-Patient Matching Platform and Multimodal Biorepository. *J. Park. Dis.* **10**, 301–313 (2020).
4. Tadel, F., Baillet, S., Mosher, J. C., Pantazis, D. & Leahy, R. M. Brainstorm: A User-Friendly Application for MEG/EEG Analysis. *Comput. Intell. Neurosci.* **2011**, 1–13 (2011).
5. Donoghue, T. *et al.* Parameterizing neural power spectra into periodic and aperiodic components. *Nat. Neurosci.* **23**, 1655–1665 (2020).
6. John, C. R. *et al. M3C: Monte Carlo reference-based consensus clustering*. http://biorxiv.org/lookup/doi/10.1101/377002 (2018) doi:10.1101/377002.
7. da Silva Castanheira, J., Orozco Perez, H. D., Misic, B. & Baillet, S. Brief segments of neurophysiological activity enable individual differentiation. *Nat. Commun.* **12**, 5713 (2021).
8. Goetz, C. G. *et al.* Movement Disorder Society-sponsored revision of the Unified Parkinson's Disease Rating Scale (MDS-UPDRS): Scale presentation and clinimetric testing results: MDS-UPDRS: Clinimetric Assessment. *Mov. Disord.* **23**, 2129–2170 (2008).
9. Nasreddine, Z. S. *et al.* The Montreal Cognitive Assessment, MoCA: A Brief Screening Tool For Mild Cognitive Impairment: MOCA: A BRIEF SCREENING TOOL FOR MCI. *J. Am. Geriatr. Soc.* **53**, 695–699 (2005).
10. Yeo, B. T. T. *et al.* The organization of the human cerebral cortex estimated by intrinsic functional connectivity. *J. Neurophysiol.* **106**, 1125–1165 (2011).

11. Hoehn, M. M. & Yahr, M. D. Parkinsonism: onset, progression, and mortality. *Neurology* **17**, 427–427 (1967).

12. Goetz, C. G. *et al. Movement* Disorder Society Task Force report on the Hoehn and Yahr staging scale: Status and recommendations The *Movement* Disorder Society Task Force on rating scales for Parkinson's disease. *Mov. Disord.* **19**, 1020–1028 (2004).

13. Markello, R. D. *et al. neuromaps: structural and functional interpretation of brain maps*. http://biorxiv.org/lookup/doi/10.1101/2022.01.06.475081 (2022) doi:10.1101/2022.01.06.475081.

14. Hansen, J. Y. *et al. Mapping neurotransmitter systems to the structural and functional organization of the human neocortex*. http://biorxiv.org/lookup/doi/10.1101/2021.10.28.466336 (2021) doi:10.1101/2021.10.28.466336.